temperatures, that is, pairs of associated positive and negative ion vacancies. We agree with Laurence's point of view because we found that the diffusion behavior of negative ion vacancies could be explained by the simple volume diffusion theory in the high-temperature region and therefore the assumption of the existence of the diffusion along disordered interfaces was not necessary. On the other hand, we are inclined to believe that the diffusion along disordered interfaces is predominant at low temperatures.

It would be very interesting to continue these experiments on crystals of varying dislocation and grain boundary structures. The exact determination of the relationship between the behavior of the diffusion and the defects in the crystals is still left to future investigations.

Note added in proof. After this work was completed, a paper on Cl ion diffusion was published by Barr, Hoodless, Morrison, and Rudham, Trans. Faraday Soc. **56**, 697 (1960). The authors are indebted to Dr. Y. Haven for this information.

Dynamics of Radiation Damage*

J. B. Gibson, A. N. Goland,† M. Milgram, and G. H. Vineyard
Brookhaven National Laboratory, Upton, New York
(Received July 14, 1960)

Radiation damage events at low and moderate energies (up to 400 ev) are studied by machine calculations in a model representing copper. Orbits of knock-on atoms are found and the resulting damaged configurations are observed to consist of interstitials and vacancies. Thresholds for producing permanently displaced atoms (i.e., interstitials) are about 25 ev in the $\langle 100 \rangle$ direction, 25 to 30 ev in the $\langle 110 \rangle$ direction, and around 85 ev in the $\langle 111 \rangle$ direction. Collision chains in the $\langle 100 \rangle$ and $\langle 110 \rangle$ directions are prominent; at low energies the chains focus, at higher energies they defocus. Above threshold, the chains transport matter, as well as energy, and produce an interstitial at a distance. The range of $\langle 110 \rangle$ chains has been studied in detail. Localized vibrational modes associated with interstitials, agitations qualitatively like thermal spikes, ring annealing processes, and a higher energy process somewhat like a displacement spike have been observed. Replacements have been found to be very numerous.

The configurations of various static defects have also been studied in this model. The interstitial is found to reside in a "split" configuration, sharing a lattice site with another atom. The crowdion is found not to be stable, and Frenkel pairs are stable only beyond minimum separations, which are found to be very much dependent on orientation.

1. INTRODUCTION

THE initial event in the damaging of a crystal lattice by high-energy radiation is the sudden transfer of a rather large amount of kinetic energy (10 to perhaps 10^5 ev) to a single atom. The energized atom then ploughs through the lattice knocking other atoms from their sites and leaving a damaged region behind. From a theoretical standpoint this damaging event is a complex many-body problem, and it has been treated in the past only by making drastic approximations.[1] Generally it has been considered as a cascade of independent, two-body collisions between knock-on atoms and stationary atoms. The knock-on atoms have been assumed to move freely between collisions. The stationary atoms have been assumed to behave as though randomly located, and their binding in the lattice has been taken into account by the very

much simplified assumption that they will be displaced and enter the group of freely moving knock-ons if and only if endowed with energy above a certain threshold, generally in the neighborhood of 25 ev. On this cascade model the damage is predicted to be a set of interstitial atoms and an equal number of vacant lattice sites, distributed randomly over a small region. Other models have been proposed in which many-body effects are given prominence. Thermal spike and displacement spike models are of this character. In the former, the region around the site of a knock-on is assumed to behave as if suddenly heated, and its subsequent cooling is treated by the classical laws of heat conduction in a homogeneous medium. In the displacement spike models, qualitative arguments about the character of damage are advanced on the assumption that a kind of miniature "explosion" occurs around the site of the knock-on. These models are difficult to harmonize with one another, and each has obvious shortcomings. Patchwork attempts at improving the models in individual details have not yet been very impressive.

In the last few years a number of sophisticated radiation damage experiments have been made. In the most notable of these highly purified metals have been

---

[1] For reviews see F. Seitz and J. S. Koehler, in *Solid-State Physics*, edited by F. Seitz and D. Turnbull (Academic Press, Inc., New York, 1956), Vol. 2, p. 305; also G. J. Dienes and G. H. Vineyard, *Radiation Effects in Solids* (Interscience Publishers, Inc., New York, 1957).

bombarded in a variety of ways at very low temperatures, and the recovery of the specimens induced by careful annealing has been studied.[2–6] Such experiments have shown that damage under even the simplest conditions still has a complex character, and controversies over its nature have increased, rather than decreased, in vigor.[7–10]

For these reasons a more realistic calculation of some typical damage processes is highly desirable. It has seemed to us that analytical methods are inadequate and that numerical treatment with the aid of a high-speed computing machine is required.[11] This paper is the first full length report on results to date.[12] Our procedure is to consider a crystallite containing a reasonably large number of atoms which interact with realistic forces. Atoms on the surface of the crystallite are supplied with extra forces simulating the reaction of atoms outside, as though the crystallite were embedded in an infinite crystalline matrix. A radiation damage event starts with all atoms on their lattice sites and all but one at rest. That one atom is initially endowed with arbitrary kinetic energy and direction of motion, as though it had just been struck by a bombarding particle. A high speed computer then integrates the classical equations of motion for the set of atoms, showing how the initially energized atom (the knock-on) transfers energy to neighboring atoms, how the dynamic stages evolve, and how the kinetic energy finally dies away and the atoms of the set come to rest in a damaged configuration. A series of "runs" are made, corresponding to a representative variety of initial conditions.

[2] J. K. Redman, T. S. Noggle, R. R. Coltman, and T. H. Blewitt, Bull. Am. Phys. Soc. 1, 130 (1956); R. R. Coltman, T. H. Blewitt, C. E. Klabunde, and J. K. Redman, Bull. Am. Phys. Soc. 4, 135 (1959); T. H. Blewitt, Symposium on Vacancies and Point Defects, Harwell (1958).

[3] H. G. Cooper, J. S. Koehler, and J. W. Marx, Phys. Rev. 97, 599 (1955); G. D. Magnuson, W. Palmer, and J. S. Koehler, Phys. Rev. 109, 1990 (1958).

[4] J. W. Corbett, J. M. Denney, M. D. Fisk, and R. M. Walker, Phys. Rev. 108, 954 (1957); J. W. Corbett, R. B. Smith, and R. M. Walker, Phys. Rev. 114, 1452 (1959); 114, 1450 (1959).

[5] J. W. Corbett and R. M. Walker, Phys. Rev. 115, 67 (1959).

[6] C. J. Meechan and A. Sosin, Phys. Rev. 113, 422 (1958).

[7] A. Seeger, Proceedings of the Second United Nations International Conference on Peaceful Uses of Atomic Energy, Geneva, 1958 (United Nations, Geneva, 1958), Paper No. 998.

[8] Proceedings of the Lattice Defects in Noble Metals Conference, edited by J. A. Brinkman, J. Meechan and A. Sosin, North American Aviation Report NAA-SR-3250 (Office of Technical Services, Department of Commerce, Washington, D. C.).

[9] National Academy of Sciences Report, Perspectives in Materials Research (to be published).

[10] C. J. Meechan, A. Sosin, and J. A. Brinkman, Phys. Rev. 120, 411 (1960)

[11] Calculations of the threshold energy for producing a permanently displaced atom have been made by H. B. Huntington [Phys. Rev. 93, 1414 (1954)], for copper, and by W. Kohn [Phys. Rev. 94, 1409 (1954)], for germanium. These treatments necessarily relied on numerous assumptions.

[12] Brief preliminary reports have been given in the following places: J. Appl. Phys. 30, 1322 (and cover) (1959). In this report [100] should be replaced by [010]; G. H. Vineyard, J. B. Gibson, A. N. Goland, and M. Milgram, Bull. Am. Phys. Soc. 5, 26 (1960), and the next three abstracts; Brookhaven National Laboratory, Annual Report, July 1, 1959 (Office of Technical Services, Department of Commerce, Washington, D. C.), pp. 12–14.

The computer program can also be used to study the stability, energy, equilibrium configuration, and other properties of lattice defects permitted by the model. One guesses the positions of the atoms in the defect and uses these as initial conditions, with zero initial velocities (actually a very small kinetic energy may be imparted to one atom to spoil the symmetries of the starting configuration). The computing machine then shows how the lattice relaxes, and with dissipation of energy at the boundary of the crystallite, aided, when desired, by artificial damping, an equilibrium configuration is eventually reached. Concurrently with the study of dynamic damage events a study of point defects has been undertaken. These are of interest in themselves, they give an independent check on the adequacy of the model, and they assist in interpreting the dynamic results.

All of the calculations made to date are for metallic copper. This material has been chosen because it is a reasonably simple metal and because more radiation damage experiments at low temperatures have been performed on it than on any other substance. It has seemed advisable to treat this one material very thoroughly before extending the calculations to other substances. The effect of a finite temperature during bombardment could, in principle, be put into the calculations by supplying small initial agitations to all the atoms. Doing this properly would require averaging over a large set of initial agitations and would enormously extend the number of computations required. Most of the annealing effects can, we feel, be sufficiently well estimated by calculating activation energies for migration of the defects and applying the theory of absolute rate processes in solids. Thus all calculations made to date have been for bombardments at a temperature of absolute zero.

A further important limitation of the calculations must be pointed out. Because of the speed and the size of memory of the computing machine available, the fundamental crystallite dealt with has been of modest size. Most of the computations reported were on crystallites containing about 500 atoms; a few computations have been done more recently on crystallites of about 1000 atoms. The forces applied to the atoms bounding the crystallite are admittedly somewhat inaccurate, and this renders the calculations less certain when boundary atoms receive large displacements during the crucial stages of a run. To avoid this it is necessary to limit the kinetic energy of the knock-on atom. Our most energetic events have been at 400 ev, and the majority of runs have been at energies an order of magnitude lower than this. The calculations are thus pre-eminently concerned with threshold and near-threshold events; many inferences for the high-energy events typical of reactor neutron bombardment can be drawn, but we are not yet able to extend the machine calculations to cover these fully.

A detailed discussion of the model and the force laws

is given in Sec. 2. Section 3 outlines the scheme of integration and the computational procedure. Section 4 describes the results of some static calculations on the defects supported in the model. Those defects are described that are necessary to an understanding of the dynamic results; a more complete report on static calculations will be given in a future paper. Section 5 reports the principal dynamic results achieved to date, and Sec. 6 summarizes the conclusions reached. In the Appendix, there is a table of all the dynamic events that have been run.

2. THE MODEL

All computations have been made on a model designed to represent metallic copper. The atoms are allowed to interact with two-body, central repulsive forces. For these a Born-Mayer form is assumed, the interaction energy of a pair of atoms at separation r being

$$\varphi = Be^{-\beta r}. \tag{1}$$

This interaction describes the repulsion of atoms at close approach. The choice of the constants in this law will be discussed below. A cohesive tendency is also needed, and for this a constant inward force is applied to each atom on the boundary of the crystallite. In the equilibrium configuration this force just balances the Born-Mayer repulsions of neighboring atoms. The equilibrium configuration, of course, is a face-centered cubic array with the normal lattice spacing of copper. Since all crystallites considered are rectangular parallelepipeds, for an atom in a face the surface force is normal to the face, for an atom in an edge the force is normal to the edge (along $\langle 110 \rangle$) and for an atom in a corner it is along the inwardly directed cube diagonal. In any distortion involving small displacement of surface atoms these surface forces give an increment of total binding energy proportional to the increment of volume of the crystallite. The forces can thus represent any binding energy that is a function only of volume of the crystallite and which varies at the right rate with volume to equilibrate the Born-Mayer repulsions. In a monovalent metal the conduction electrons are the major source of binding, and their cohesive energy is, to a certain approximation, dependent only on volume. Thus the constant surface forces employed here represent, in first approximation, the cohesive effect of the conduction electrons. This combination of two-body repulsions plus constant surface forces is easy to apply in machine computation, it gives a crystallite which, at equilibrium, has no distortions near the surface, and it would seem to be at least as faithful to the forces in a real metal as any two-body force law with a repulsive core and attractive tail (Morse potentials, Lennard-Jones potentials, etc.) that can be devised. Since it is not a purely central-force model, it does not require the Cauchy relation for the elastic constants.

Since the crystallite is supposed to behave as a set of atoms on the interior of an infinite perfect crystal, it is necessary to have additional forces on the surface atoms to represent the reaction forces of atoms beyond the surface caused by any displacement of atoms in the microcrystallite. For small displacements an elegant expression for these reactions can be written in terms of a Green's function and an integral over the history of the motions in the crystallite. It does not seem feasible to use this expression in an actual calculation, however, both because of the difficulty of finding the Green's function explicitly and because of added requirements on storage of information during the computation. Instead, the additional surface forces were simply taken to be a spring force, proportional to the displacement of the surface atom, and a viscous force, proportional to the velocity of the surface atom. These are only approximations to the true reaction forces, but with judicious choice of the spring and viscosity constants, they are thought to be adequate for the accuracy required. The spring forces represent the tendency of material just outside the crystallite to resist slow or static deformation of the crystallite by a system of forces proportional to the deformation.

The spring constants were arrived at by the approximate arguments that follow: The crystallite is first replaced by a sphere of equal volume, embedded in an infinite homogeneous, elastic medium with isotropic elastic properties. If the sphere is expanded from radius R to $R+\delta R$ the equations of elasticity show that a pressure P acts on the surface of the sphere, and

$$P = (4\mu/R)\delta R, \tag{2}$$

where μ is the shear modulus of the medium. The effective normal spring force on each atom at the surface of the crystallite is found by dividing P by the number of atoms per unit area in a cube face. The shear modulus is taken to be c_{44}, as determined from the Born-Mayer potential φ used in Eq. (6) below. The effective normal spring force per atom, so determined, is proportional to δR. The normal part of the effective spring constant, k_n, is then taken to be this force for unit displacement δR. Static tangential displacements of a surface atom are assumed to be resisted by a tangential force, given by a tangential effective spring constant, k_t. To calculate k_t we consider a long right circular cylinder of radius R, embedded in an infinite homogeneous medium with isotropic elastic properties. If this cylinder is rotated about its axis so that the tangential displacement of a point on its surface is δR, a shear stress is set up with magnitude $\mu\delta R/R$ at the surface. Distributing this equally over surface atoms in the same manner as before, one finds that the tangential displacement of each atom in the surface is opposed by a force proportional to that displacement. Thus one finds $k_t = \frac{1}{4}k_n$.

These spring constants are smaller by a factor of the order of a/R (a is the lattice constant) than the constants that would be obtained by holding the atoms beyond the surface fixed while displacing a surface atom. Physically, this factor allows for the tendency of atoms beyond the surface to move in cooperation with the motion of a surface atom and thus to oppose its motion less strongly than if they were fixed.

The spring forces on surface atoms are conservative, and it is essential to have surface dissipations, which will allow the large energies introduced into the crystallite by a primary knock-on to disappear. If disturbances reach the surface with small amplitude they can be analyzed there into harmonic plane waves, and if the surface were treated rigorously it would absorb these waves with no reflection. Using only viscous damping on the

surface it is not possible to absorb all waves perfectly. As the best compromise we ask that a normally incident wave of selected frequency be absorbed as well as possible. We have chosen the viscosity coefficient for motion of a surface atom perpendicular to the surface so as to give the maximum possible absorption for a normally incident plane wave of longitudinal polarization and of half the maximum frequency of such waves. Also we have chosen the viscosity coefficient for motion of a surface atom parallel to the surface so as to give maximum possible absorption for a normally incident wave of transverse polarization and of half the maximum frequency of such waves. The criterion for maximum absorption is easy to find since a plane wave normally incident on a plane boundary presents a one dimensional problem. Under the present conditions it is found that the reflection coefficient (for power) at the mid-frequency is about 0.02; at the maximum frequency and at zero frequency the coefficient is unity, but drops steeply from these extremes and averages about 0.28 over the entire range of frequencies.

The above account has shown how the two spring force constants and two viscosity constants for each atom in the flat faces of the crystallites were chosen. The atoms in the corners and edges of the crystallite were given spring and viscosity constants derived from these by the rather obvious device of superimposing the constants associated with each face in which the atom was simultaneously resident.

These crude criteria for choosing force constants are best justified by experience with the calculations. Results have not proved very sensitive to boundary effects, as is demonstrated by cases where the same dynamic event has been run twice, starting at a different point in the crystallite, and where the same event has been run both in a large and in a small crystallite. Comments on these happenings will be made subsequently.

Choice of a size and shape for the microcrystallite is a matter of balancing the need to keep strong action away from the boundaries against the increased computing time required by a larger set of atoms. Except for a few special trials all runs to date have been made in three fundamental microcrystallites, which will be referred to as sets A, B, and C. All were rectangular parallelepipeds bounded by {100} planes. Set A was
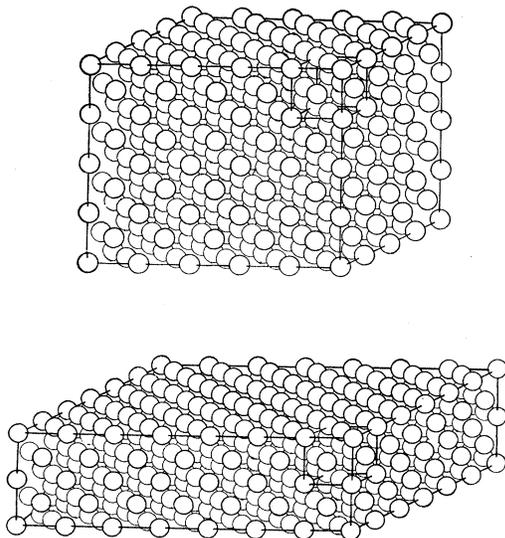
FIG. 1. Two of the sets of atoms used in the calculations. Set A is above, Set B is below.

made up of 5×4×4 unit cells, and contained 446 atoms. Set B was 2×6×7 unit cells, and contained 488 atoms. Set C was 2×9×10 unit cells and contained 998 atoms. To standardize the descriptions an origin of a cartesian coordinate system will always be located in a corner of the set, and the x, y, and z directions will always be the same. All lengths are measured in such units that the cubic unit cell of copper has length 2. The range of starting positions of atoms in the various sets are then given in Table I.

Sets A and B are pictured in Fig. 1. Set A has been used for a variety of shots at odd directions. Sets B and C have been used only for shots with initial knock-on velocity in the (100) plane. The initial knock-on was always in the plane $x=2$, which appears to be sufficiently far away from the boundaries $x=0$ and $x=4$, and the larger y and z dimensions of these sets allowed more energetic events to be contained.

The Born-Mayer form of repulsive potential, Eq. (1), was chosen largely after the lead of Huntington[13,14] and Seitz[13] in work on point defects and self diffusion in face centered cubic metals. It is admittedly an approximation, but it is hoped that it may be an adequate approximation over the range of distances important to the present problem if the constants B and β are properly chosen. At very close approach, potentials of interaction can be established on theoretical grounds, and at separations near the equilibrium separation in the crystal some information is available from considerations of elastic constants and from atom-atom scattering experiments that have been conducted in gases. The radiation damage problem, unfortunately, demands knowledge of the potential at intermediate separations, where no reliable information exists. We have attempted to bridge this gap in the following way: We have three Born-Mayer potentials, which will be referred to simply by number, all of which give a moderately good account of the elastic constants and their variation with pressure when employed near equilibrium separations, and which are plausible as extrapolations to large separations of the theoretical repulsive potentials at small separation. The difference between the three potentials shows most strongly in the threshold energy for permanent displacement of an atom by irradiation, and the choice among the three is ultimately made by comparison between the calculated and measured threshold energy.

TABLE I. Characteristics of fundamental sets.

Set	Range of initial atomic positions	Number of atoms
A	$0 \leq x \leq 10$, $0 \leq y \leq 8$, $0 \leq z \leq 8$	446
B	$0 \leq x \leq 4$, $0 \leq y \leq 12$, $0 \leq z \leq 14$	488
C	$0 \leq x \leq 4$, $0 \leq y \leq 18$, $0 \leq z \leq 20$	998

[13] H. B. Huntington and F. Seitz, Phys. Rev. 61, 315 (1942).
[14] H. B. Huntington, Phys. Rev. 91, 1092 (1953).

TABLE II. Constants in the Born-Mayer potentials employed [see Eq. (3)].

Potential	A (ev)	ρ
1	0.0392	16.97
2	0.0510	13.00
3	0.1004	10.34

Figure 2 shows various curves of repulsive potential energy between a pair of copper atoms plotted against the separation of the pair. At separations smaller than 0.1 A the screened Coulomb potential suggested by Bohr,[1] $\varphi = Z^2 e^2 r^{-1} \exp(-r/\alpha)$, where $\alpha = a_0 2^{-\frac{1}{2}} Z^{-\frac{1}{3}}$, Z being the atomic number, e the charge of the electron, and a_0 the Bohr radius, is a good representation. At larger separations the Bohr potential is undoubtedly too small.[15] Theoretical potentials which should be better than the Bohr potential at moderately small separations and which agree with the Bohr potential at very small separations have been found by Abrahamson,[16] using the Thomas-Fermi and the Thomas-Fermi-Dirac approximations (labeled TF and TFD, respectively, in Fig. 2). The TFD curve is probably the more accurate of the two. Both of these become unreliable at about 1 A, and so the curves are terminated a little beyond this point. The three Born-Mayer potentials employed in the present work are the three straight lines, labeled Pot. 1, Pot. 2, and Pot. 3. Potentials 1 and 2 are close to those suggested by Huntington for copper. For energies in the range 1- to 100-ev potential 2 represents a smaller atom than potential 1. Potential 3 was chosen arbitrarily to give the same bulk modulus as potential 1 and to give, at intermediate energies, the smallest atom of the three. It is seen from Fig. 2 that any of the three potentials might be joined to the TFD curve between 100 and 1000 ev by moderate alterations in the range 10 to 100 ev, although this would require the least alteration if done with potential 2, and would produce a more complex curve if done with potential 1. Allowing for a considerable uncertainty in the TFD result, no one of the potentials 1 to 3 is immediately ruled out for the low and moderate energy range, although potential 2 looks best. It will be shown subsequently that all three potentials give qualitatively similar results, both for the static configurations of lattice defects and for dynamic damage events, but that the threshold energies for producing a permanently displaced atom are very different for the three, being too high for potential 1, too low for potential 3, and approximately

FIG. 2. Various forms of repulsive potential energy for a pair of copper atoms. Potentials 1, 2, and 3 were used in the calculations. r_0 is the equilibrium separation in the crystal.

right for potential 2. The majority of our calculations have been made with potential 2.

To specify the potentials it is convenient to recast Eq. (1) into a commonly used form,

$$\varphi = A \exp[-\rho(r-r_0)/r_0], \qquad (3)$$

where r_0 is the near neighbor distance at zero pressure and absolute zero of temperature. Taking r_0 for copper to be 2.551 A, the constants A and ρ for the potentials employed in the present work are given in Table II.

The contribution of the repulsive force to the elastic moduli can be computed from the formulas[17]

$$c_{11}' = 2^{\frac{1}{2}} r_0^{-1} [\varphi'' + r_0^{-1} \varphi'], \qquad (4)$$

$$c_{12}' = 2^{-\frac{1}{2}} r_0^{-1} [\varphi'' - 5 r_0^{-1} \varphi'], \qquad (5)$$

$$c_{44}' = 2^{-\frac{1}{2}} r_0^{-1} [\varphi'' + 3 r_0^{-1} \varphi'], \qquad (6)$$

$$B = (c_{11} + 2 c_{12})/3, \qquad (7)$$

where primes on φ denote derivatives, evaluated at $r = r_0$, and only contributions from nearest neighbors have been considered. B is the bulk modulus. The complete elastic constants are the above expressions augmented by contributions from the conduction

[15] See J. A. Brinkman, J. Appl. Phys. 25, 961 (1954). Measurements of ranges of knock-on atoms also confirm this conclusion. See R. A. Schmitt and R. A. Sharp, Phys. Rev. Letters 1, 445 (1958), and D. K. Holmes and G. Leibfried, J. Appl. Phys. 31, 1046 (1960).

[16] A. A. Abrahamson, thesis, New York University, 1960 (unpublished); A. A. Abrahamson, R. D. Hatcher, and G. H. Vineyard, Bull. Am. Phys. Soc. 5, 231 (1960).

[17] H. B. Huntington, in Solid-State Physics, edited by F. Seitz and D. Turnbull (Academic Press, Inc., New York, 1958), Vol. 7, p. 213.

TABLE III. Elastic moduli[a] (units 10^{11} dynes/cm^2).

	c_{11}	c_{12}	c_{44}	B
Potential 1	14.5	10.0	6.3	11.5
Potential 2	10.9	8.1	4.5	9.0
Potential 3	13.2	10.9	5.2	11.6
Experiment, 0°K	17.6	12.5	8.2	14.2

[a] First three rows list Born-Mayer part of moduli, as given by Eqs. (4)–(7). Experimental values from W. C. Overton, Jr., and J. Gaffney, Phys. Rev. 98, 969 (1955).

electrons and from Coulomb interactions of the ion cores.[17] The simplest possible estimate of the electronic contribution treats the conduction electrons as free and neglects the strain dependence of the energy of the bottom of the conduction band. In this way a contribution to the bulk modulus and to c_{11} and c_{12} of 6.4×10^{11} dynes/cm^2 is predicted. If an effective mass for electrons of $1.47 m_0$ is assumed, this contribution drops to 4.3×10^{11} dynes/cm^2. The free electron contribution to these moduli must, in our model, be allotted to the surface forces. The third elastic modulus, c_{44}, is not directly affected by the Fermi energy of conduction electrons; Fuchs calculated that for copper the electrostatic interaction of the ions with the conduction electrons should contribute 2.6×10^{11} dynes/cm^2 to c_{44}. Table III lists the values of the contributions to elastic moduli from the various Born-Mayer potentials employed here, and also the experimental elastic moduli for copper at 0°K.

Table III shows that an electron contribution to the bulk modulus of about 2.6×10^{11} dynes/cm^2 is needed with potentials 1 and 3 and about 5.2×10^{11} dynes/cm^2 is needed with potential 2. These contributions would also bring c_{11} and c_{12} approximately to the experimental values. Electron contributions of this magnitude are reasonable, in view of estimates mentioned above, but exact values are difficult to establish. This contribution could be brought into our model by additional spring forces on the boundary. The spring forces already employed act in this direction, but are too small to contribute appreciably to the effective elastic constants. The dynamic stages of a damage event clearly would not be affected by such changes; experience with the computations leads us to believe that the static results also would not be very much affected, since most of the distortion around interstitials and vacancies is large near the defect, but very small at the boundary of the crystallite. More work is needed, however, to establish this point fully.

The value of c_{44} that comes from the Born-Mayer forces also is small compared with the experimental value, and an electrostatic effect such as that calculated by Fuchs is needed. This shortcoming of our model would not be expected to affect the dynamic stages of damage events appreciably, but it may affect the stability of lattice defects. Because of this and also because of the lack of any other special energies

associated with electron rearrangement near lattice defects, our model may not give correct stability and energy for all defects. The argument for pursuing calculations in great detail with this model is that it will provide one complete and self-consistent picture of both the damage process and the ensuing lattice disruption. Corrections to the model can then be made as a second approximation.

3. METHOD OF COMPUTATION

A. Integrating the Equations of Motion

Solving a large number of coupled differential equations is time consuming, even on a high speed computer. Since the force law employed is only an approximation to the true force law, it was deemed not worthwhile to strive for extremely high accuracy in the integration scheme; instead, a simple central difference procedure was used which gives reasonable accuracy along with reasonable speed.

Let the ith atomic coordinate at time t be $x_i(t)$ and let the associated velocity be $v_i(t)$, where $i = 1, 2, \cdots N$ and N is three times the number of atoms in the crystallite. The force in the ith degree of freedom depends, in general, on the positions of all atoms. In the case that x_i refers to a boundary atom the force depends in addition on the velocity in the ith degree of freedom (because of the viscous damping). Thus the force may always be written $F_i[x_1(t), \cdots x_N(t); v_i(t)]$. Letting m be the mass of an atom, the classical equations of motion of the system are

$$\dot{v}_i(t) = m^{-1} F_i[x_1(t), \cdots x_N(t); v_i(t)], \qquad (8)$$

$$\dot{x}_i(t) = v_i(t), \quad i = 1, 2, \cdots N. \qquad (9)$$

Our procedure is to replace time derivatives by finite differences with arbitrary interval Δt; coordinates are defined on integer steps and velocities on half integer steps:

$$\dot{v}_i(t) \cong [v_i(t + \Delta t/2) - v_i(t - \Delta t/2)]/\Delta t, \qquad (10)$$

$$\dot{x}_i(t + \Delta t/2) \cong [x_i(t + \Delta t) - x_i(t)]/\Delta t. \qquad (11)$$

In Eq. (9) t is replaced by $t + \Delta t/2$, then (10) and (11) are inserted in (8) and (9). Rearrangement gives[18]

$$v_i(t + \Delta t/2) \cong v_i(t - \Delta t/2) + \Delta t m^{-1} F_i[x_1(t), \cdots x_N(t);$$
$$\times v_i(t - \Delta t/2)], \qquad (12)$$

$$x_i(t + \Delta t) \cong x_i(t) + \Delta t v_i(t + \Delta t/2), \quad i = 1, 2, \cdots N. \qquad (13)$$

Starting with a complete set of positions $x_i(t)$ at arbitrary time t, and corresponding velocities $v_i(t - \Delta t/2)$, the machine essentially employs (12) to compute the new velocities $v_i(t + \Delta t/2)$ and (13) to compute new coordinates $x_i(t + \Delta t)$. The process is then iterated to generate coordinates at $t + 2\Delta t$, $t + 3\Delta t$, etc.,

[18] There is a minor inconsistency in that the viscous force in (12) is computed from $v_i(t - \Delta t/2)$. This introduces no appreciable error.

together with the corresponding velocities. The optimum size for Δt depends on the maximum velocity of any atom. Thus in the early stages of a calculation Δt is small; after the velocities of moving atoms have diminished, Δt may be increased to hasten the computation. The calculation is stopped whenever the configuration is judged to have stabilized sufficiently. Considerations governing the choice of Δt are discussed below. The program itself will be described in detail in a forthcoming Brookhaven National Laboratory report.

The coordinates and velocities of all atoms at alternate time steps are stored on magnetic tape and can be printed out as desired. The positions of selected atoms can also be displayed as dots on a cathode-ray screen. Displays are presented sequentially and multiflash pictures, such as Figs. 14 and 15, can be taken on stationary film; by advancing the film after each display, moving pictures have been made.

B. Units Used in the Calculation

For convenience the unit of length was chosen to be one-half a cubic cell edge of Cu,

$$l_0 = 1.804 \times 10^{-8} \text{ cm},$$

the unit of time was such that a 1000-ev copper atom would have unit velocity,

$$t_0 = 3.273 \times 10^{-15} \text{ sec},$$

and the unit of energy was one electron volt,

$$E_0 = 1.602 \times 10^{-12} \text{ erg}.$$

From these one obtains the unit velocity (v_0) as 5.512×10^6 cm/sec and the unit of mass $m_0 = E_0/v_0^2 = 5.275 \times 10^{-26}$ g, which is 1/2000 the mass of a copper atom.

C. Energy Checks

The central difference scheme employed in the present calculation leads to a rigorous conservation law, analogous to the energy conservation principle of classical mechanics and reducing to the latter when $\Delta t \rightarrow 0$. To demonstrate this, one first notes, from two applications of Eq. (13), that

$$v_i(t+\Delta t/2)+v_i(t-\Delta t/2)$$
$$= (\Delta t)^{-1}[x_i(t+\Delta t)-x_i(t-\Delta t)]. \quad (14)$$

Rewriting Eq. (12), one has

$$m[v_i(t+\Delta t/2)-v_i(t-\Delta t/2)]$$
$$= \Delta t F_i[x_1(t),\cdots x_N(t); v_i(t-\Delta t/2)]. \quad (15)$$

Multiplying Eq. (14) by Eq. (15), one finds

$$(m/2)[v_i^2(t+\Delta t/2)-v_i^2(t-\Delta t/2)]$$
$$= F_i[x_1(t),\cdots x_N(t); v_i(t-\Delta t/2)]$$
$$\times \tfrac{1}{2}[x_i(t+\Delta t)-x_i(t-\Delta t)]. \quad (16)$$

This relation shows that the increase of kinetic energy in the ith degree of freedom in one time step is rigorously equal to an effective work done during that time step. The effective work is seen to be the product of the force at time t by an averaged displacement $(\tfrac{1}{2})[x_i(t+\Delta t)-x_i(t-\Delta t)]$. This displacement may also be written $(\tfrac{1}{2})[x_i(t+\Delta t)+x_i(t)]-(\tfrac{1}{2})[x_i(t)+x_i(t-\Delta t)]$, which shows that it is the increment in average position associated with time t. Equation (16) may be written for each time step, summed over the time steps from starting time 0 to time $T=M\Delta t$, and summed again over all degrees of freedom. This gives the master conservation law

$$K(T)-K(0)=-[\Phi(T)-\Phi(0)]-D(T). \quad (17)$$

Here $K(T)$ is the total kinetic energy of the system at time T,

$$K(T) = (m/2) \sum_{i=1}^{N} v_i^2(T+\Delta t/2). \quad (18)$$

$\Phi(0)-\Phi(T)$ is a version in finite differences of the work done on the system by all conservative forces, and $D(T)$ is essentially the dissipative work in the interval 0 to T. Φ might be termed a pseudopotential. If the force F_i is divided into a conservative part F_i^c (the Born-Mayer plus the spring forces) and a dissipative part F_i^d (the viscous force), one has

$$\Phi(T)-\Phi(0) = -\sum_{i=1}^{N} \sum_{\mu=1}^{M} F_i^c[x_1(\mu\Delta t),\cdots x_N(\mu\Delta t)]$$
$$\times \frac{[x_i(\mu\Delta t+\Delta t)-x_i(\mu\Delta t-\Delta t)]}{2}, \quad (19)$$

and

$$D(T) = -\sum_{i=1}^{N} \sum_{\mu=1}^{M} F_i^d[v_i(\mu\Delta t-\Delta t/2)]$$
$$\times \frac{[x_i(\mu\Delta t+\Delta t)-x_i(\mu\Delta t-\Delta t)]}{2}. \quad (20)$$

If $\Delta t \rightarrow 0$ $\Phi(T)$ approaches the classical potential energy $V(x)$, where $-\partial V(x)/\partial x_i = F_i^c$, and x is the coordinate set at time T.

The following use has been made of the conservation law (17). The kinetic energy K, and the cumulative dissipation (to surface viscosity) D, are computed at each time step. Equation (17) is then employed to compute the pseudopotential Φ. The classical potential $V(x)$ is also computed directly from its analytic form and compared with Φ at each stage. If the difference is less than a preset tolerance the machine proceeds automatically to the next time step; if the difference exceeds the tolerance, the machine repeats the calculation of the present time step. If the difference is now within tolerance the machine proceeds, if it is again outside tolerance the machine stops. A large class

of possible machine errors will cause a discrepancy beyond tolerance, and in the automatic repetition of the step the error may be rectified. Truncation errors (inadequacy of the finite difference approximation) also will cause a discrepancy between Φ and V, and thus the energy check monitors errors of this kind as well. Tolerance is usually kept at about 1.0 ev when Φ and V are in the vicinity of 125 ev (sets A and B). It is felt that this is sufficient accuracy. When the truncation error proves to be larger than this, the calculation is restarted with a smaller value of Δt. All of the energies are printed out on line for each time step; this shows the progress of the calculations, and also gives, at the end, the stored energy of the defect configuration produced.

D. Choice of Δt

The choice of an optimum interval Δt is a matter of some delicacy. Analytic solutions of the finite difference equations for one-dimensional problems with certain simplified potentials can be found, and these give useful insight. In general the force must not vary by too large a fraction of itself in one time step. This means that in an actual calculation, the pair of atoms with strongest interaction anywhere in the system places the most severe demand on Δt, and our choice of Δt has generally been governed by the energy in the strongest interaction. During stages of vibration at small amplitude, on the other hand, the system is behaving as a set of coupled oscillators. The analytic solution of the simple harmonic oscillator problem shows that Δt must be small compared with the period of the oscillator, and we have interpreted this to mean that the coupled oscillator problem requires Δt to be small compared with the shortest normal period of the system.

Ultimately, the only reliable check on Δt is afforded by repeating a calculation with a smaller Δt and comparing the results. This has been done on selected test problems. The problem shown in Fig. 8 (25 ev in the (100) plane, 15° away from [010]) was run with three different time steps, 2, $\frac{1}{2}$, and $\frac{1}{8}$, and the first collision was checked in detail for each. This collision takes place between times 4 and 8, which is only two time steps in the case of the largest Δt. Positions and velocities during the collision differed only in the fourth place in the case of $\Delta t = \frac{1}{2}$ and $\frac{1}{8}$. The calculation with $\Delta t = 2$ differed, at most, in the second place from the results with $\Delta t = \frac{1}{8}$. It was concluded that for this collision $\Delta t = \frac{1}{2}$ was small enough, reduction to $\Delta t = \frac{1}{8}$ being unnecessary. It is surprising that $\Delta t = 2$, sampling the collision in only two steps, gave an error of but 1% in position. The energy transfer to the atom struck in the collision was about 3% higher for $\Delta t = 2$ than for $\Delta t = \frac{1}{8}$. Following experience of this kind, the following procedures were developed: Problems with initial energies around 25 ev were regularly started with $\Delta t = 1$, those with initial energy around 100 ev were

started with $\Delta t = \frac{1}{2}$, and those with initial energies around 400 ev were started with $\Delta t = \frac{1}{4}$. After energy checks had been built into the program, these values of Δt were reduced by a factor of two so that the larger discrepancies in energy occurring only during collisions would not stop the program.

As the collision cascade proceeds the energy of a moving atom is divided about in half at each collision. As this energy decreases Δt may be increased. The upper limit for Δt is determined by the frequency of the localized modes of the split interstitials. This is perhaps 2.5 times the Debye frequency. The Debye period is about 70 time units, the period of the localized mode is about 24. In order to describe this mode there should be several time steps per quarter cycle, and thus $\Delta t \cong 2$ is the maximum. All other modes are below the Debye frequency and permit $\Delta t \cong 6$. This largest time step has been used in some static problems.

E. Computational Speed

With 500 atoms the computing time required for one time step is about one minute on the IBM 704. The program is such that this time is proportional to the number of atoms. Total time to run a problem to quiescence varies a great deal. In some problems the end point is reasonably certain after about an hour. More ambitious problems, in which the settling down is followed in detail, require considerably more time. The history of such a problem will be described, to give an idea of fairly typical procedures. The problem is shown in Fig. 13, and was a shot at 35 ev, in the (100) plane, directed 1° away from [010], in set B (488 atoms). From $t = 0$ to 23, Δt was taken as $\frac{1}{2}$ (46 steps). Δt was then increased to 1 for $t = 23$ to 82 (59 steps). Next Δt was increased to 2 and the problem was run from $t = 82$ to $t = 182$, (50 steps). At this time the motions were very small; Δt was increased to 6 and the run was continued to $t = 566$ (64 steps). The total was 219 steps, or a little over three and one half hours of machine time. Miscellaneous operations such as setting up tapes, taking edits, and making movies might require one half to one hour more.

F. Reliability

Errors may be divided into truncation error, round off error and machine errors. Truncation errors were discussed in the section on the choice of Δt, machine errors in the energy check section. Round off error would not seem to be important, since the equivalent of eight decimal places is carried by the machine. This would make truncation error much more important, by several orders of magnitude. Before energy checks were built into the system results were checked for physical reasonableness. Most problems contained some symmetry, and errors were detected by the loss of this property. Several problems were also run twice to check reliability. Even with our built in energy check,

energies, positions, and velocities are checked for reasonableness whenever possible. It is believed that all large errors have been detected by these means.

4. STATIC RESULTS

It is desirable to know the configuration and stability of various lattice defects that can be housed in our model. Accordingly a number of "static" calculations have been run. In these the equilibrium configuration of a defect is estimated from simple considerations, and the atoms are given these coordinates at the beginning. All the atoms are started from rest, except that in cases where the configuration has symmetry one atom is given a very small initial velocity in such a way as to spoil the symmetry without introducing appreciable kinetic energy. False equilibria corresponding to "dead center" positions are thus avoided. The machine calculates the motions of the atoms from these initial conditions, until a static, equilibrium configuration is reached. Artificial damping (in which the kinetic energies of all atoms are set equal to zero each time the total kinetic energy reaches a maximum) is usually employed to hasten the attainment of equilibrium.

A full report on the static results will be presented in a future paper. In this section enough information will be given to aid in interpreting the dynamic calculations.

The vacancy seems entirely normal.[19] All three potentials have been employed, and in the case of potentials 2 and 3 the calculations have been run long enough to come very close to equilibrium. The behavior is qualitatively similar in all three cases, with the amount of relaxation being largest in the case of potential 3 and least with potential 1. The nearest neighbors relax radially inward by a small amount—about 1.5% of the equilibrium distance, $\sqrt{2}$, in the case of potential 1; 2.5% in the case of potential 2; and 3.2% in the case of potential 3. The second neighbors, and more distant neighbors in or near the cubic axial directions, relax slightly outward. In the case of second neighbors, the percentage outward relaxation is about one twentieth the inward relaxation of near neighbors. Such apparently anomalous relaxation has already been found by others[20] and is easily understood by considering the geometry of the lattice. An immediate consequence is that the strain field at a distance from the vacancy cannot be very well fitted to the field of a point singularity in an *isotropic* elastic continuum. A cubic elastic continuum is required and the outward relaxation along cubic directions can be

FIG. 3. The split configuration of the interstitial that is found to be stable. Relaxation of neighbors not shown.

considered as a manifestation of the anisotropic character of the medium.[21]

The interstitial has been investigated carefully with potential 2, and is found not to reside at the center of the cubic unit cell. Instead, the interstitial has what may be termed a split configuration, in which it shares a lattice site symmetrically with another atom, the axis of the pair being along a cubic axis of the lattice. Figure 3 shows a split interstitial in the face-centered lattice. For potential 2 the separation of the two atoms is very nearly 1.2 (in units in which the lattice constant is 2). The possibility of this configuration of the interstitial in copper was pointed out by Huntington and Seitz,[12] although its stability was not settled at that time. More recently, Johnson et al.[22] have also demonstrated its stability in a lattice model rather similar to ours. It should be noted that there are three possible orientations of this interstitial on each lattice site; its symmetry is only tetragonal, and it should thus give rise to resonant anelastic effects.

The stability of this interstitial has been demonstrated in two calculations. First an interstitial was set up in the cube center, with relaxations of its neighbors, according to our first estimate of the stable position of the interstitial. The machine calculation showed that this atom rapidly moved away from the cube center toward a neighboring atom, in a direction determined by minor asymmetries in the starting conditions, and settled down in the split configuration with this atom. Later, as a check, the split configuration, with minor perturbations, was set up as an initial condition, and a long machine run was made. This demonstrated the complete stability of the split configuration and gave accurate values of the relaxations of surrounding atoms. As will be seen in the following section, a number of dynamic events have also produced interstitials (see, for example, Figs. 12 and 13), and in all cases these are seen to settle down in the split configuration.

[19] Our results give no support to the "relaxion" picture of the vacancy which has been put forward by N. H. Nachtrieb and G. S. Handler, Acta Met. 2, 797 (1954), and N. H. Nachtrieb, H. A. Resing, and S. A. Rice, J. Chem. Phys. 31, 135 (1959).
[20] H. Kanzaki, J. Phys. Chem. Solids 2, 24 (1957); G. L. Hall, J. Phys. Chem. Solids 3, 210 (1957); A. Seeger and E. Mann, J. Phys. Chem. Solids 12, 326 (1960); L. A. Girifalco and V. G. Weizer, J. Phys. Chem. Solids 12, 260 (1960).

[21] The writers are indebted to Dr. E. Kröner and Dr. A. Seeger for information on strain fields of point sources in a cubic elastic medium. Quantitative comparisons with Kröner's solutions will be given in a future paper.
[22] R. A. Johnson, G. H. Goedecke, E. Brown, and H. B. Huntington, Bull. Am. Phys. Soc. 5, 181 (1960).

The foregoing calculations do not demonstrate fully that there are no other stable configurations of the interstitial, and indeed experimental evidence has occasionally been interpreted as requiring that the crowdion be stable in copper. We have tested the stability of the crowdion in our model by two static calculations, both employing potential 2. In both of these a crowdion was formed by inserting an interstitial atom in a $\langle 110 \rangle$ line and moving three atoms on either side of the inserted atom outward along the line by diminishing amounts. A total of eight neighbors on adjoining $\langle 110 \rangle$ lines were also relaxed away from the interstitial, in each case, to obtain the lowest energy configuration possible. In one calculation the extra atom was inserted half way between two neighboring lattice sites and the relaxation along the line was made symmetrical about this point. This might be called a space-centered crowdion. In the second calculation, which might be called a site-centered crowdion, the extra atom was placed on one side of a lattice site and the pattern of relaxation was made symmetrical about this site. Both crowdions proved to be unstable, and decayed into a split interstitial by simple rotation of a pair of atoms near the center. The decay occurred rather slowly, however, which demonstrates that the potential energy is fairly flat near these crowdion configurations. We conclude that the crowdion is not stable in our model; nevertheless, rather modest changes in the force laws might make it stable.

It is also necessary to know which Frenkel pairs are stable. Accordingly a series of static runs on Frenkel pairs at various separations were made with potential 2. The results for pairs in the {100} plane are shown in Fig. 4. Here the split interstitial is shown at a fixed position in the lower left corner of the figure. Lattice sites around this interstitial at which a vacancy
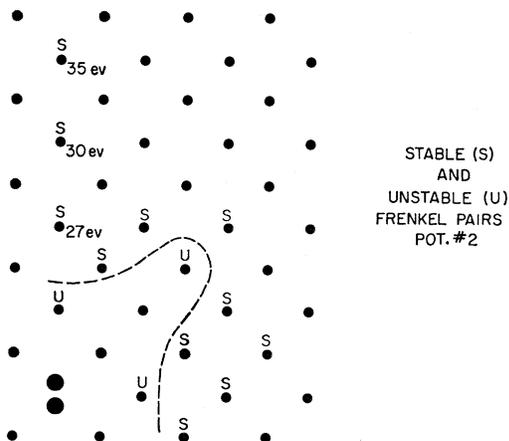
FIG. 4. Stability of Frenkel pairs in {100} plane of copper. Split interstitial is at lower left. Dotted line separates stable from unstable sites for a vacancy. Approximate threshold energies for dynamic production of three particular pairs are indicated.

yielded a stable Frenkel pair (by actual calculations) are indicated by S. Sites for the vacancy which yielded an unstable Frenkel pair are indicated by U. All sites inside the dotted line are unstable, all sites outside it are stable. It is seen that a surprisingly large separation of the pair is needed to produce stability, particularly for a pair on a close packed line. The size of this region of instability has obvious implications for near-threshold damage events, and also for the annealing process in which a migrating interstitial recombines with a vacancy.

Energies associated with various point defects are also under investigation, and a very brief account will be given here. Let W_v be the work needed to take an atom reversibly from a normal lattice site to a distant point out of the crystal. Let W_I be the work needed to take an atom from this distant point and to insert it, reversibly, into a perfect crystal, forming a split interstitial. In our model, W_v is given by the potential energy of the perfect crystallite, minus the potential energy of the crystallite containing a thoroughly relaxed vacancy. Similarly W_I is the potential energy of the crystallite containing a relaxed split interstitial, minus the potential energy of the perfect crystallite. W_v and W_I include the potential energies of the surface forces. For potential 2, static runs give

$$W_v = -0.71 \text{ ev,}$$
$$W_I = 3.38 \text{ ev.}$$

To appreciate the significance of these numbers, one must consider that the thermodynamic energy of formation of a vacancy, E_v, and energy of formation of an interstitial, E_I, are related to W_v and W_I by

$$E_v = W_v - W_s,$$
$$E_I = W_I + W_s,$$

where W_s is the work needed to take an atom reversibly from an average site on the surface of the crystal to a remote point outside the crystal. E_v and E_I are the energies that determine the equilibrium concentrations of vacancies and interstitials, in the familiar way. Since our model does not give a proper account of a free surface it is not convenient to compute W_s directly. Instead one can consider the work needed to disassemble the entire crystal, after cutting off the surface forces at a suitable finite range. This work, per atom, will also be an estimate of the sublimation energy, W_s; such considerations show that, in our model, W_s is negative. Reasonable values of W_s give reasonably good values of E_v and E_I, although the latter tends to lie lower than expected.

The energy of formation of a separated Frenkel pair, E_F, is given by

$$E_F = E_v + E_I = W_v + W_I = 3.38 - 0.71 = 2.67 \text{ ev.}$$

This is lower than values indicated by some earlier

calculations,[23] but is not entirely outside reasonable limits.

The divacancy and trivacancy have been studied in a preliminary way with potential 2, and have configurations generally consistent with findings of other investigators.[24,25] The binding energy of the divacancy, against separation into isolated vacancies, is about 0.06 ev in our model, and of the trivacancy, against separation into three isolated vacancies, is about 0.5 ev. These binding energies are lower than those reported in the literature.[24,25] Work on these energies, on activation energies for migration, and on other clusters of point defects is continuing.

5. DYNAMIC RESULTS

We come now to the chief results of this work, dynamic problems corresponding to real radiation damage events. To date about 45 distinct calculations leading to usable results have been run. These have involved all three of the repulsive force laws (see Fig. 2), a rather wide variety of knock-on directions, and a number of knock-on kinetic energies up to 400 ev. In this section, a representative selection of the dynamic events will be discussed. These events have been chosen to give a good general idea of what has been learned, without attempting to discuss details of every event run. In the Appendix Table IV lists all the events run successfully, and Fig. 5 is a diagrammatic presentation of all of the events in which potential 2 was used for the repulsive force (for discussion see below). As will be seen the dynamic events give strong preference to

FIG. 5. Diagram showing all dynamic events calculated with potential 2 (see also Appendix). A dot is shown for each event, and indicates kinetic energy and direction of knock-on atom. First figure attached gives number of stable Frenkel pairs created, figure in parenthesis gives number of replacements. Dotted line is estimated threshold for creation of at least one stable Frenkel pair.

[23] Huntington,[13] found 5 to 6 ev for E_F. Radiation damage experiments have yielded 5.4 ev[6] and also much lower values.[2]
[24] J. H. Bartlett and G. J. Dienes, Phys. Rev. **89**, 848 (1953).
[25] A. C. Damask, G. J. Dienes, and V. G. Weizer, Phys. Rev. **113**, 781 (1959).

FIG. 6. Atomic orbits produced by shot in (100) plane at 40 ev. Knock-on was at A and was directed 15° above $-y$ axis. Large circles give initial positions of atoms in plane; small dots are initial positions in plane below. Vacancy is created at A, split interstitial at D. Run to time 99. (Run No. 12).

potential 2 among the three forms tried. Consequently this one has been used for most of the calculations.

A. Description of Events

Figure 6 shows the trajectories resulting in the y-z plane when an atom (A) is set in motion with 40 ev of kinetic energy in a direction in this plane making an angle of 15° with the $-y$ axis. The initial positions of atoms in the planes immediately above and below the plane of major action are shown by small black dots. Large open circles show the atoms in the plane of major action at time 0, large black dots show the positions of these atoms at time 99 (one time unit is 3.27×10^{-15} sec). The large open circles give the sizes of the atoms, as determined by the distance of closest approach in a head-on collision between a 40-ev atom and a stationary atom. Atoms for which no trajectory is shown suffered negligible displacements. Replacement collisions can be seen at B and C, a vacancy is left at A, and an interstitial is formed at D. This appears to be the usual split configuration (see Fig. 3) in which the atom at $y=1$, $z=4$ is displaced upward from its lattice site, the site being shared by D. Also notable are the chains of strongly focused collisions along $\langle 110 \rangle$ and $\langle 100 \rangle$ directions, including the chains AD, AE, FG, BH, etc. The $\langle 110 \rangle$ focusing is essentially that predicted by Silsbee[26] (see below), but the $\langle 100 \rangle$ focusing occurs only because of the influence of neighboring lines of atoms, and had not been anticipated. Atoms along all lines other than AD are in the process of relaxing back to the vicinity of their original positions. Although the relaxation has not

[26] R. H. Silsbee, J. Appl. Phys. **28**, 1246 (1957).

TABLE IV. Table of dynamic events calculated.

Run number	Potential (see Fig. 2)	Direction of knock-on	Kinetic energy of knock-on (ev)	Set (see Table I)	Coordinates of knock-on atom[a]	Final time[b]	Number of replacements	Number of displacements (Frenkel pairs)	Remarks[c]
4	1	[100]	25	A	2,4,4	23	0	0	Below threshold. Two knock-ons in this run.
4	1	22½° from [100][d]	25	A	8,4,4	23	0	0	Below threshold. Two knock-ons in this run.
2	1	[111]	25	A	4,4,4	18	0	0	Below threshold. See Fig. 20.
14	3	[111]	20	A	2,2,2	92	0	0	Atom does not reach cube center. Below threshold. Two knock-ons in this run. See Fig. 19.
15	3	[111]	23	A	2,2,2	258	0	0	Atom does not reach cube center. Below threshold. Two knock-ons in this run. See Fig. 19.
15	3	[1̄11]	27	A	8,6,2	258	0	0	Atom reaches cube center but returns. Below threshold. Two knock-ons in this run. See Fig. 19.
17	3	[1̄11]	27	A	8,6,2	130	0	0	Same as 27 volt atom in run No. 15. Confirms run 15.
14	3	[1̄11]	30	A	8,6,2	92	2	0	Struck atom goes to cube center. Static calculations indicate it is unstable and will decay by 2 replacements. Two knock-ons in this run.
16	3	[1̄11]	30	A	8,6,2	200	2	0	Same as 30-volt atom in run No. 14, but carried to longer time. Confirms No. 14. See Fig. 19.
18	3	[111]	100	A	2,2,2	45	2	1	At end of run, interstitial is in cube center at 7,7,7. Must make split interstitial in this cell. Vacancy left at 2,2,2. Δt=4, which is rather large.
39	2	[100]	20	A	2,4,4	175	0	0	Temporarily forms split interstitial around 4,4,4, oriented along [100]. This is unstable and reverts to original configuration.
30	2	[010]	25	B	2,2,6	380	1 (est)	1 (est)	Appears to be making interstitial at 2,6,6, oriented along [010]. Vacancy is at 2,2,6. Stability is not quite certain. Machine error about t=180.
46	2	[100]	25	A	2,4,4	47	1 (est)	1 (est)	Confirms No. 30 as far as it goes.
54	2	1° from [010][d]	30	B	2,2,6	317	2	1	Makes split interstitial at 2,8,6, oriented along [010]. Vacancy left at 2,2,6. See Fig. 12.
50	2	1° from [010][d]	35	B	2,2,6	566	3	1	Makes split interstitial at 2,10,6 oriented along [010]. Vacancy left at 2,2,6. See Fig. 13.
72	2	1° from [001][d]	50	B	2,5,1	75	5	1	Should make split interstitial either at 2,5,13, or 2,5,15 with vacancy at 2,5,1. See Fig. 14.
73	2	1° from [001][d]	100	B	2,5,1	42	10 (est)	1 (est)	Defocusing chain gives maximum KE of 59 ev to atom at 2,5,11. Should make interstitial at about 2,5,21 with vacancy at 2,5,1. See Fig. 15.
31	2	5° from [010][d]	25	B	2,2,6	250	5 (est)	0 (est)	At end has made split interstitial at 2,5,5, oriented along [001]. May decompose by 5-membered ring mechanism. (See No. 25.)
91	2	15° from [010][d]	23	B	2,2,6	199	0	0	Below threshold.
25	2	15° from [010][d]	25	B	2,2,6	646	5	0	Forms split interstitial at 2,5,7, vacancy at 2,2,6, then decomposes by 5-membered ring mechanism. Δt=2 up to t=442. See Figs. 8–11.
35	2	15° from [010][d]	25	B	2,2,6	22	5 (est)	0 (est)	Δt=0.125, for check on truncation error in No. 25.

[a] Coordinates are relative to origin at corner of set, with axes oriented as in Table I.
[c] Estimated positions of some defects are outside atomic set used.
[b] In units of 3.273×10⁻¹⁶ sec.
[d] In (100) plane.
[e] In (01̄1) plane.

TABLE IV. Continued.

Run number	Potential (see Fig. 2)	Direction of knock-on	Kinetic energy of knock-on (ev)	Set (see Table I)	Coordinates of knock-on atom[a]	Final time[b]	Number of replacements	Number of displacements (Frenkel pairs)	Remarks[e]
35A	2	15° from [010]^d	25	B	2,2,6	51	5 (est)	0 (est)	Δt=0.5, for check on truncation error in No. 25.
12	2	15° from [0̄10]^d	40	A	3,6,5	99	2	1	Interstitial formed at 3,1,4, oriented along [001]. Vacancy at 3,6,5. Two knock-ons in this run. See Fig. 6.
32	2	22½° from [010]^d	25	B	2,2,6	114	0	0	Below threshold.
12	2	22½° from [010]^d	40	A	7,2,3	99	4 (est)	1 (est)	Interstitial estimated to be forming at about 7,7,8, orientation uncertain. Vacancy at 7,2,3. Two knock-ons in this run. See Fig. 7.
40	2	[011]	25	B	2,2,2	44	?	?	Cannot run long enough to determine whether above threshold. See Fig. 16.
44	2	[011]	100	B	2,2,2	27	135 (est)	1 (est)	Dynamic crowdion. See Fig. 17.
45	2	[011]	400	B	2,2,2	14	600 (est)	1 (est)	Dynamic crowdion. See Fig. 18.
74	2	1° from [011]^d	25	B	2,2,2	78	?	?	Cannot run long enough to determine whether above threshold.
75	2	1° from [011]^d	50	B	2,2,2	54	45 (est)	1 (est)	Dynamic crowdion. See No. 95.
95	2	Continuation of No. 75		B	2,1,1 and near neighbors	46	...	...	Displacements and velocities of all near neighbors of atom 2,11,11 of No. 75, at time 36 in that problem, were used as starting conditions for atom 2,1,1 and near neighbors in this problem.
76	2	1° from [011]^d	100	B	2,2,2	33	?	?	Collision chain is defocusing. Atom at 2,10,10 acquires 59 ev.
71	2	10° from [011]^d	50	B	2,2,2	92	10 (est)	1	Interstitial estimated to form at about 2,13,13. Vacancy is at 2,2,2. See Fig. 22.
62	2	10° from [011]^d	100	B	2,2,2	130	11 (est)	2 (est)	Interstitials appear to be formed at about 2,11,11 and 2,0,10, vacancies at 2,2,2 and 2,4,6. See No. 96.
96	2	10° from [011]^d	100	C	2,6,8	703	12	2	Repeat of No. 62 in larger set. Interstitials form and stabilize at 2,14,18 (along [001]) and 2,3,17 (along [010]). See Figs. 23 and 24.
63	2	10° from [011]^d	400	B	2,2,2	15	12	2	Estimates of end point are very crude because large energies reach boundary. See No. 97.
97	2	10° from [011]^d	400	C	2,6,8	45	39 (est)	11 (est)	Repeat of No. 63 in larger set. See Fig. 25.
10	2	[1̄11]	25	A	8,6,2	78	0	0	Below threshold. Note dual excitation. See Fig. 20.
34	2	[111]	35	A	2,2,2	31	2 (est)	0	Struck atom goes to cube center at 3,3,3. Decay in two membered ring is expected.
10	2	[111]	40	A	2,2,2	78	2 (est)	0 (est)	Struck atom goes to cube center at 3,3,3. Decay by two membered ring is expected. Note dual excitation. See No. 33 and Fig. 20.
33	2	[111]	40	A	2,2,2	66	2 (est)	0 (est)	Single knock-on, to check No. 10. Gave same behavior of 40-ev knock-on as No. 10.
69	2	[111]	60	A	2,2,2	141	2 (est)	0 (est)	Struck atom is near 3,3,3 at end of run. This is expected to decay by two membered ring. See Fig. 21.
70	2	[111]	100	A	2,2,2	49	1	1	Vacancy left at 2,2,2. Interstitial will be near 5,5,5 but exact location is uncertain. See Fig. 21.
42	2	20° from [100]^e	25	A	2,4,4	86	0	0	Below threshold.
43	2	30° from [100]^e	25	A	2,4,4	70	0	0	Below threshold.
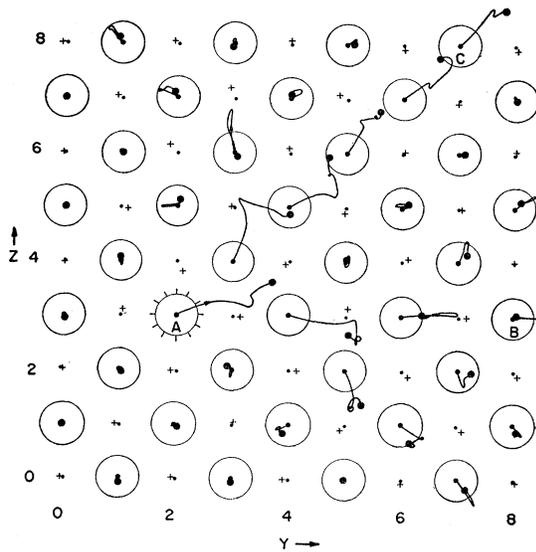
FIG. 7. Similar to Fig. 6 except that knock-on (A) is directed $22\frac{1}{2}°$ above y axis. Small crosses show positions of atoms in plane below at end of calculation (time 99). Vacancy is left at A, interstitial is estimated to form near C (Run No. 12).

been entirely completed by time 99, experience with this and other events convinces us that the further relaxation will not change the topology of the final configuration from that which is evident in Fig. 6. The net result of this event is two replacements and one Frenkel pair. Although velocities are not given in Fig. 6, it should be noted that a great range of velocities occurs. The original knock-on, which had 40 ev at A, has slowed to 19 ev just before A' (where it is in nearly head-on collision with B), and has dropped to only 0.1 ev just beyond the point A'.

Figure 7 shows an event similar to that in Fig. 6, but different in detail. Atom A was initially projected in the y-z plane with a kinetic energy of 40 ev but at an angle of $22\frac{1}{2}°$ with the y axis. The large circles and large black dots indicate initial positions and positions at time 99, respectively, as in Fig. 6. The small black dots indicate initial positions of atoms in the planes just above and below, the small crosses indicate positions in these adjacent planes at time 99. A focusing chain AB is again seen, but atoms in this chain are returning to their original sites, while a chain of replacements occurs in the diagonal direction AC, and an interstitial is being formed somewhere along this chain, most likely at the site $y=7$, $z=8$ (but possibly at $y=6$, $z=7$). The orientation of this interstitial is in doubt, and cannot be reliably determined by running the calculation longer because the displacement of the boundary atom C has become large and assumptions employed in the boundary forces are brought into question. A vacancy is clearly left at A, one Frenkel pair has been created, and four replacements appear to have occurred. The disturbance in adjacent planes, as shown by the crosses in the figure,

is surprisingly slight. This is the case with all our events in which the initial velocity lies in a {100} plane. Comparing Figs. 6 and 7 it is noteworthy how much difference in location of the interstitial is caused by a small change in the direction of initial motion. The qualitative similarity of focusing tendencies in the two figures is also evident. More will be said below about focusing.

The preceding events were well above the threshold for production of lattice defects. An event very near threshold (actually, as it turns out, just below threshold) will be discussed next. An atom at 2,2,6, was given 25 ev of kinetic energy in a direction 15° from the y axis and lying in the y-z plane. Figure 8 shows the trajectories of atoms in this plane (the plane $x=2$) from time 0 to time 128. In this and in the next two figures, trajectories are indicated by dotted lines. Successive dots are separated by two units in time, so speeds along the trajectories can be estimated from the spacing of the dots. The struck atom was initially at the site indicated by the large circle. Figure 9 shows the same plane of atoms between times 130 and 254, and Fig. 10 shows the plane between times 256 and 380. In Fig. 8 a replacement is seen to occur at 2,4,6 and this atom is forced into the split interstitial position around the site 2,5,7. Prominent focusing chains are seen to branch off along several close packed lines. These transport energy, but not matter, away from the scene of initial action. In Fig. 9 the split interstitial is better established and the organized motion in the focused chains has begun to disperse. In Fig. 10 the kinetic energy has died away further and the vacancy and interstitial are clearly evident. Because of the localized vibrational modes associated with the vacancy and interstitial, particularly with the latter, there is still an appreciable amount of kinetic energy in and near the interstitial.
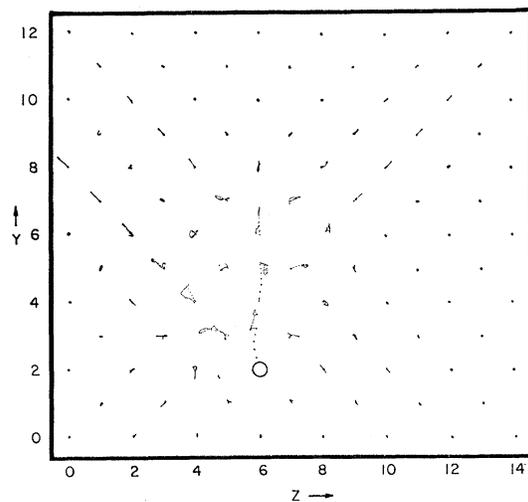
FIG. 8. Orbits produced in (100) plane by 25-ev knock-on (large circle) directed 15° away from y axis. Atomic positions at intervals of 2 units in time are shown. Orbits are shown from time 0 to 128 (Run No. 25).

As has been noted before this particular Frenkel pair is stable in our model, but very precariously so, and when the event we have been discussing was carried to still longer times, the kinetic energy retained near the defect caused a self-annealing. This occurred by means of a ring interchange involving five atoms and the five sites 2,2,6; 2,4,6; 2,5,7; 2,4,8; and 2,3,7; the orbits of these atoms during the complete run from time 0 to 646 are shown in Fig. 11. Times at various points along the orbits are indicated by numbers in the figure. The configuration evident in Fig. 10 is beginning to drift between time 300 and time 400. Between 400 and 500 the two members of the split interstitial are developing a more pronounced motion, and shortly after time 500 the two atoms at 2,4,8 and 2,3,7 are pushed along so that the former replaces the latter and the latter falls into the vacancy. By time 646 the atoms are very near their new lattice sites, from which they will obviously not escape again. The results of this shot are thus 5 replacements and no permanent displacements.

Inspection of Fig. 11 shows how a truly cooperative motion of several atoms can be involved in some annealing processes. It is also plausible that localized vibrational modes associated with a defect can play an important role in trapping a portion of the initial kinetic energy near the defect, creating a local hot spot which cools more slowly than in a perfect lattice and thus enhances self-annealing. Clearly it is a matter of considerable delicacy to establish exactly what defect is created by each near-threshold event.

A series of shots with initial velocity vector near a cube axis will be considered next. In Run No. 39, the atom at 2,4,4 was given 20 ev directed along [100]. This formed a temporary split interstitial on the sites at 4,4,4, leaving a vacancy at 2,4,4. This Frenkel pair is unstable and collapses back to the original lattice after a short time. Run No. 30 was similar except that the initial
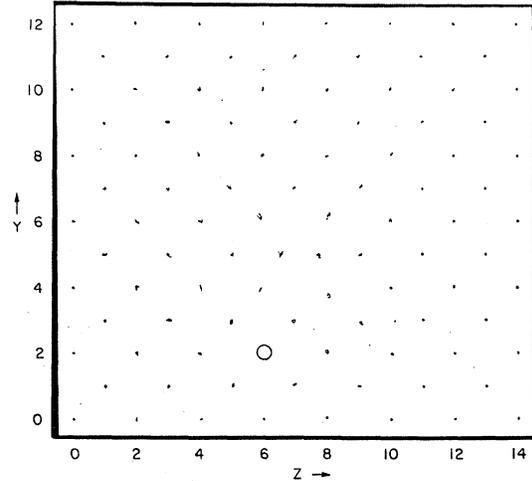
FIG. 10. Same event shown in Fig. 8, time running from 256 to 380. Temporary Frenkel pair has been produced. Note quasi-thermal agitation in vicinity of pair (Run No. 25).

energy was 25 ev. Here a split interstitial is formed 4 units away from the vacancy, a Frenkel pair that has been proved in static runs to be stable. In the dynamic run a machine error occurred at about time 180, so that
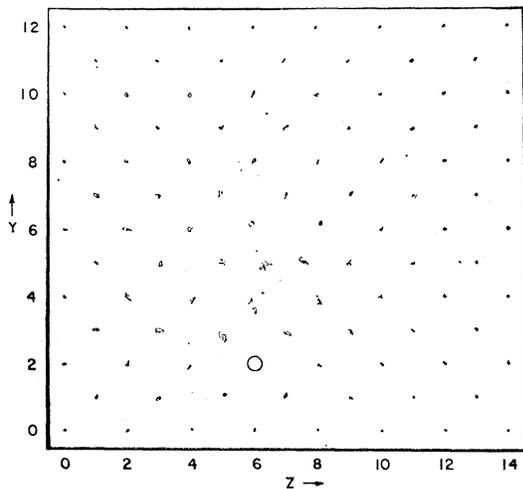
FIG. 9. Same event shown in Fig. 8, time running from 130 to 254. (Run No. 25).
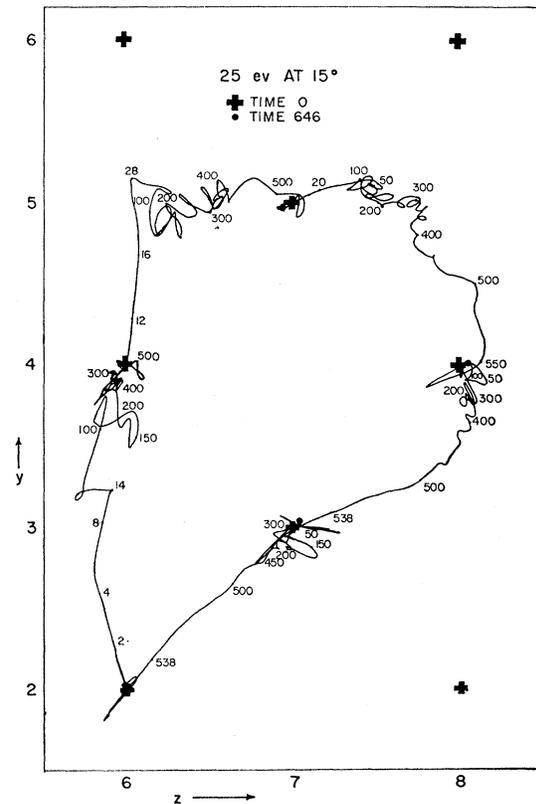
FIG. 11. Orbits of 5 atoms involved in ring interchange by which Frenkel pair seen in Fig. 10 spontaneously annealed after time 400. Figures along orbits indicate times (Run No. 25).
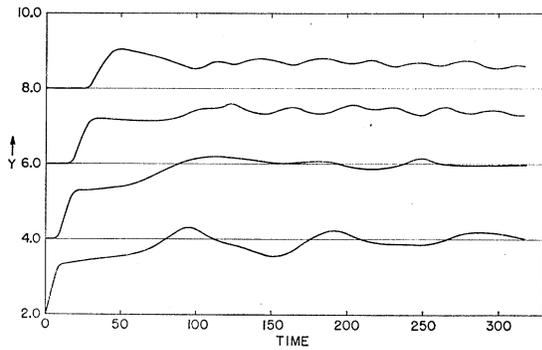
FIG. 12. y coordinates vs time for line of atoms. Knock-on (bottom curve) shot at 30 ev, 1° away from y axis. Split interstitial is created at $y=8$ (Run No. 54).

it was not possible to be quite sure that this configuration would not anneal itself before quieting down completely. The threshold for this direction is thus estimated to be very near 25 ev with our potential 2. Run No. 54 was at 30 ev, with atom 2,2,6 directed initially 1° away from the y axis in the plane $x=2$. This seems clearly to make a Frenkel pair after 2 replacements, the vacancy being left at 2,2,6 and the split interstitial, oriented along y, being centered on 2, 8, 6. Run No. 50 was exactly like No. 54 except that the initial energy was 35 ev. This time there were 3 replacements and the interstitial formed at 2,10,6. Figure 12 shows the y coordinate vs time for the replaced and displaced atoms in the 30-ev run (No. 54) and Fig. 13 shows the same information for the 35-ev run (No. 50). In Fig. 12 the localized antiphase vibration of the two members of the split interstitial is clearly evident after time 120. The period of this vibration is about 33 time units, which means that its frequency is about twice the Debye frequency for copper. Assisted focusing down the cubic axis is clearly evident in these runs, and Figs. 12 and 13 may be considered to picture the transport of both
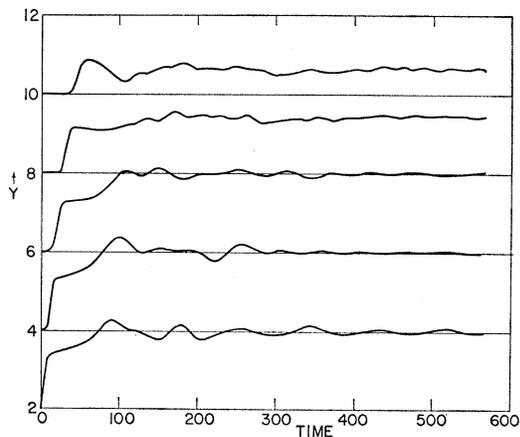
FIG. 13. y coordinates vs time for line of atoms. Knock-on (bottom curve) shot at 35 ev, 1° away from y axis. Split interstitial is created at $y=10$ (Run No. 50).

matter and energy in $\langle 100 \rangle$ chains. Similar action along $\langle 110 \rangle$ has been termed a "dynamic crowdion;"[8] and it is seen that the dynamic crowdion, if this is to be the name adopted, can indeed act along the $\langle 100 \rangle$ axes as well. The energy loss in the $\langle 100 \rangle$ case is at a greater rate than in $\langle 110 \rangle$. In runs No. 50 and No. 54 (see, e.g., the maximum slopes of the successive curves in Figs. 12 and 13) and also in runs No. 72 and No. 73 at higher energies, the attenuation of energy in well focused $\langle 100 \rangle$ chains occurs at the rate of 7 to 8 ev per collision. Atoms other than those in the direct path of the knock-ons in these events are not moved very far and return to the vicinity of their original sites.
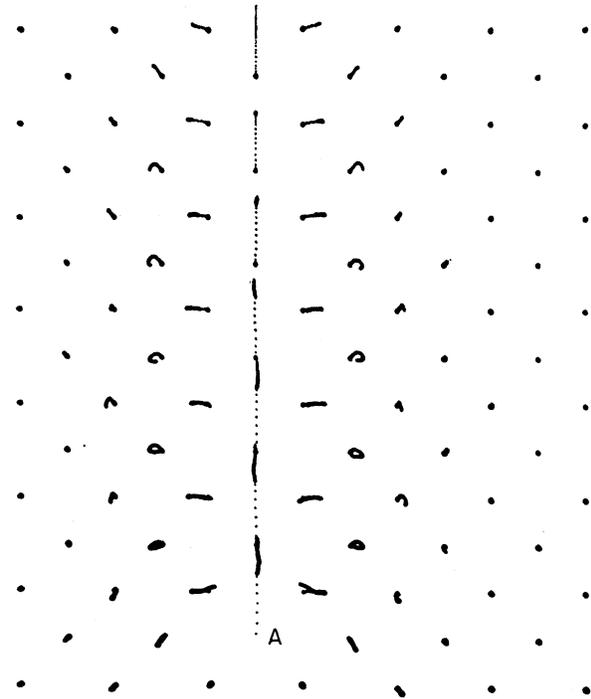
FIG. 14. Orbits in (100) plane caused by knock-on starting at A with 50 ev, initially directed 1° away from z axis. $\langle 100 \rangle$ collision chain is seen. Final time 75 (Run No. 72).

Runs No. 72 and No. 73 also had the struck atom directed in the $x=2$ plane, at an angle of only 1° from the z axis. In the former the kinetic energy was 50 ev, in the latter it was 100 ev. Orbital plots of the atoms in the $x=2$ plane are given for these runs in Figs. 14 and 15, respectively. In Fig. 14 the focusing remains good. The vacancy is left at the original site, the interstitial is projected to a point outside the original set of atoms. One estimates that the interstitial would be formed at either 2,5,13, or 2,5,15, which means 6 or 7 replacements. In Fig. 15 a pronounced early defocusing is visible (associated with the higher energy). It is estimated that about 10 replacements would occur and the interstitial would be left at about 2,5,21.

A series of shots in or near the close-packed direction

⟨110⟩ have also been made. At low energies pronounced focusing in this direction has been found, at high energies defocusing occurs, followed by focusing when the chain has lost enough energy. When directed close to ⟨110⟩ these chains lose energy only very slowly, at a rate of about 2/3 ev per collision for energies from 3 to several hundred ev. Consequently their range is so long that they cannot be stopped inside our set of atoms. Contrary to early expectations, the threshold energy for producing permanent displacements in ⟨110⟩ is rather low. Because of the difficulty with the long range of these chains, we have not been able to obtain an accurate value for this threshold, but the best estimate is that,

FIG. 16. Δz vs time for series of atoms in [011] chain. Knock-on, starting at time 0, had 25-ev kinetic energy, directed along [011] (Run No. 40).
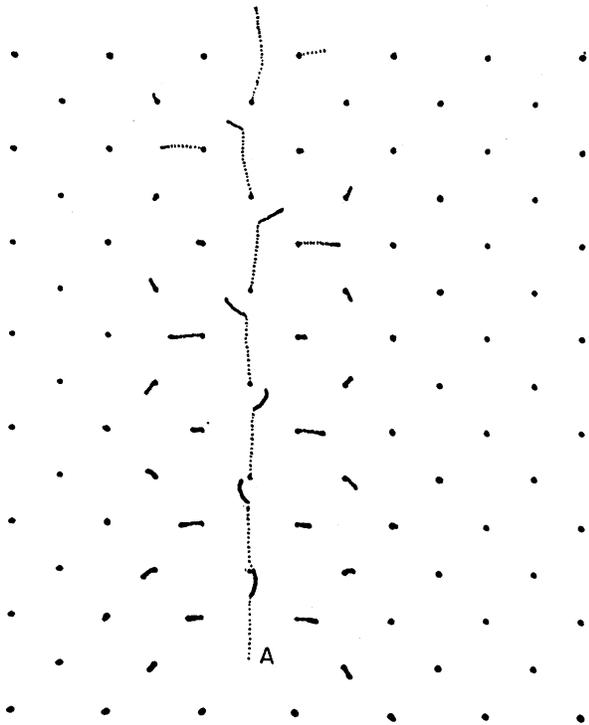
FIG. 15. Orbits in (100) plane caused by knock-on starting at A with 100 ev, initially directed 1° away from z axis. ⟨100⟩ collision chain with pronounced defocusing is seen. Final time 42 (Run No. 73).

the others, relaxes back toward its original site and will clearly return there. The anomalous behavior of this atom is explained by the fact that the atom preceding it has not moved much, and thus an unbalanced restoring force is supplied by the second atom in the chain. The second and neighboring atoms are lingering near saddle points, and it is impossible to tell for certain from this calculation whether their relaxation will finally be forward or back. In any case, a slightly higher initial energy should insure the forward relaxation, and if this occurs an interstitial must be produced some distance down the chain and a vacancy will be left at the site of the *second* atom in the chain. In some other events that have been run, it would appear that the vacancy may even form at the site of the third atom in the chain.

A higher energy event which clearly does produce a permanently displaced atom is shown in Fig. 17. This event is exactly like that of Fig. 16 except that the initial atom was given a kinetic energy of 100 ev. Now each atom moves well past the midpoint in its first strong collision, and subsequent relaxation is proceeding in a forward direction. This time the vacancy is being formed at the site of the first atom. The interstitial should be formed about 150 atomic distances away. Figure 18 shows the same thing again at a still higher initial energy, 400 ev. Results are much like the 100-ev case, with a more pronounced tendency for the entire

for potential 2, it is less than 35 ev and probably is in the neighborhood of 25 ev. Since the ⟨100⟩ threshold is also around 25 ev, this means that both of these directions are important in near-threshold bombardments. Also it is clear that the interstitial produced by a ⟨110⟩ chain will be far from the beginning of the chain—at least 10 atomic spacings near threshold and as much as 150 spacings at 100 ev. Fig. 16 gives the z-displacements versus time for successive atoms in a chain initiated at 25 ev exactly along [011]. Each atom moves just slightly past the midpoint ($\Delta z = 1/2$) between it and its neighbor, before being brought to rest, and the relaxation thereafter is extremely slow. The first atom, unlike

FIG. 17. Similar to Fig. 16, with initial kinetic energy of 100 ev. Curves belonging to consecutive atoms are identified by numbers at upper right (Run No. 44).
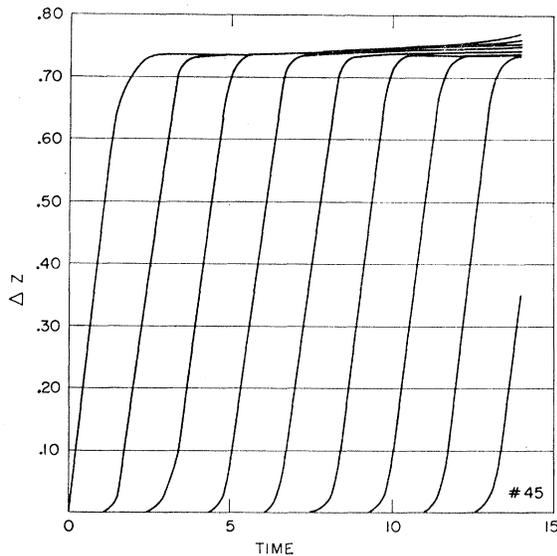
FIG. 18. Similar to Fig. 16, with initial kinetic energy of 400 ev (Run No. 45).

chain to move forward one step. In all three of these figures the high degree of preservation of energy down the chain is evident. Action of the dynamic crowdion is thus seen to occur in $\langle 110 \rangle$ as well as in $\langle 100 \rangle$.

A number of shots along $\langle 111 \rangle$ have been made. All three repulsive potentials have been used, and here the most extensive comparison of potentials two and three exists. In all cases the chains of displacements occurred in the $\langle 111 \rangle$ line, with considerable energy transferred to adjoining atoms and carried off in other chains. With enough energy the struck atom penetrates a triangle of near neighbors and lodges temporarily in the center of a unit cube. With more energy it replaces the atom at the far corner of the cube, causing this atom to lodge temporarily in the center of the next cube. With still more energy two replacements occur and the interstitial first appears at the center of the third cube. In all cases this cube center position is known, from separate static calculations, to be unstable, although these dynamic runs were not continued long enough to show it. The instability will ultimately (in times of about 200 to 400)
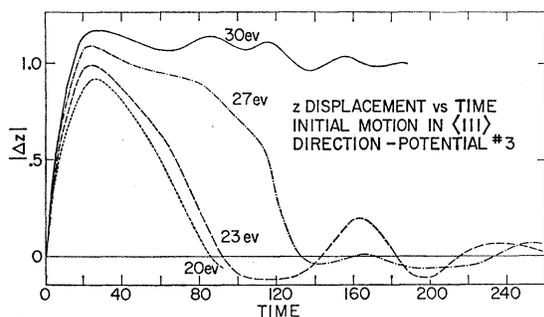
cause the interstitial at the cube center to move toward one of the six nearest lattice sites, forming a split interstitial on that site. In case the interstitial is produced in the center of the first cube, collapse of the Frenkel defect by a ring-type self-annealing mechanism must ultimately occur. In this process two replacements will occur and no defect will remain.

Figure 19 shows the z component of displacement (Δz) of the struck atom for a series of shots along $\langle 111 \rangle$ with interatomic potential number 3. Initial energies of 20, 23, 27, and 30 ev were used. The triangle of near neighbors is at $\Delta z = 2/3$; the cube center is at $\Delta z = 1$. Beyond the cube center is a second triangle of atoms at $\Delta z = 4/3$. The 20 and 23 volt shots pass a little beyond the first triangle, spreading these atoms out and also pushing them slightly ahead. The atoms of the triangle then push the struck atom back to its place of origin. With 30 ev the struck atom goes far enough through the triangle to allow the triangle to close in behind it, confining it near the center of the cube for the duration of the calculation, 200 time units. From a second calculation started quasi-statically it is known that this Frenkel pair is unstable, and will decay by a replacement process in another 100 to 200 time units. The 27-ev shot almost locks into the cube center, but drops back after time 100.

The 30-volt shot in Fig. 19 was useful for testing the adequacy of the boundary conditions employed. The struck atom was at 8,6,2 in atomic set A (see Fig. 1), and was projected in the direction $[\bar{1}\bar{1}1]$. This location is symmetric with respect to the y and z faces of the set, but not with respect to the x faces, since the x dimension of the set was 10, the y and z dimensions 8. When Δx and Δy are plotted against time and compared with Δz, it is found that Δx, Δy, and Δz remain the same to high accuracy (1 part in 10^4) until time 130, when fluctuating differences commence to occur, primarily in Δx. The velocity of longitudinal waves in this model is about 0.08 (our units). The time required for a longitudinal plane wave to travel from the struck atom to the faces $y = 0$ and $z = 8$, be reflected, and return to the struck atom is thus very close to the time when asymmetric behavior sets in, and this reinforces the belief that reflection at the boundaries is indeed responsible. The resulting asymmetry is slight, however, remaining less than 1%, which argues that reflections are not a serious disturbance to the calculations.

FIG. 19. z displacement vs time for knock-on directed along $\langle 111 \rangle$ at various energies. Potential 3 (Runs Nos. 14, 15, and 17).
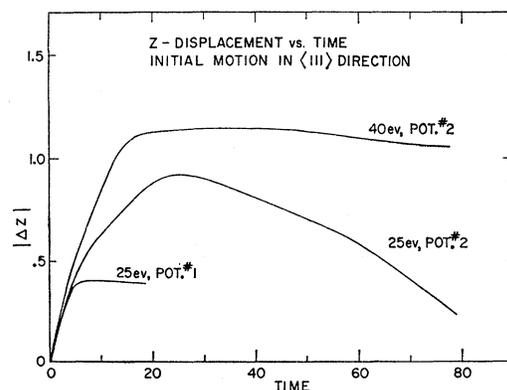
FIG. 20. Similar to Fig. 19 but with potential 1 (run No. 2) and potential 2 (run No. 10).

Figure 20 shows the z-component of displacement for more shots along $\langle 111 \rangle$, first 25 volts with interatomic potential number 1, then 25 and 40 volts with interatomic potential number 2. In the first of these the struck atom does not even penetrate the triangle of near neighbors, and is clearly returning directly to its site, even though the calculation was run only a very short time. The effect of increasing the atomic size is evident— the threshold for reaching the center of the cube has become much higher. The shot at 25 ev with potential 2 is very much like that at 20 ev with potential 3 (Fig. 19), and is also below threshold. That at 40 ev with potential 2 is like that at 30 ev with potential 3.

Two higher energy shots are shown in Fig. 21. Both involve interatomic potential 2. In both cases the struck atom was 2,2,2 and its initial motion was along [111]. Δz is plotted against time for atoms 2,2,2, 4,4,4, and 6,6,6. In one shot (dotted lines in Fig. 21) the initial kinetic energy was 60 ev, in the second (solid lines) it was 100 ev. It is seen that 60 ev is only enough to project the interstitial into the nearest cube-center position, whence it must decay by the previously mentioned mechanism, resulting in two replacements and no displacements. With 100 ev, an interstitial is created temporarily at the center of the second cube (5,5,5). In times beyond the end of the run this should produce an interstitial in the split configuration, whose exact location will be determined by any slight departures from symmetry; each of the six possible locations is known from static calculations to be stable. The threshold for production of a permanently displaced atom by a shot in the direction $\langle 111 \rangle$ (with interatomic potential 2) is thus seen to be between 60 and 100 ev, a value notably higher than for the directions $\langle 100 \rangle$ and $\langle 110 \rangle$.

The next three figures show results of some shots above threshold in a direction well away from symmetry axes, namely 10° away from [011] in the plane $x=2$. In the first of these the atomic set B was used, in the last two the large set C was used (see Table I). Orbital plots of the plane $x=2$ are shown. In all cases the

FIG. 22. Shot in (100) plane at 50 ev, 10° away from [011]. Orbits in (100) plane, to time 92, are shown. Knock-on started at A (Run No. 71).

interatomic potential was number 2. In Fig. 22 the initial kinetic energy was 50 ev. A collision chain is seen, which leaves a vacancy at its beginning (marked A) and is about to produce an interstitial after perhaps 10 replacements. The transition from a defocused to a focused condition is evident in this chain. Figure 23 shows a 100-ev shot (No. 96) which, because of the large set in which it was run is completely contained. Time runs up to about 200 units in this figure. The knock-on atom was at V_1. Two vacancies are created, at V_1 and V_2, and
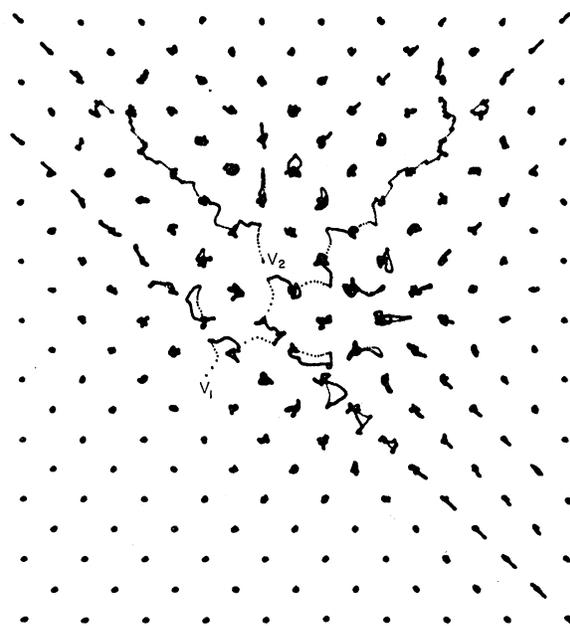
FIG. 23. Shot in (100) plane at 100 ev, 10° away from [011]. Orbits in plane to time 200 (approximately) are shown. Knock-on started at V_1 (Run No. 96).

FIG. 21. Two $\langle 111 \rangle$ shots at higher energies with potential 2. Δz vs time is shown for several atoms. Dotted lines, knock-on energy 60 ev (Run No. 69); solid line, knock-on energy 100 ev (Run No. 70).
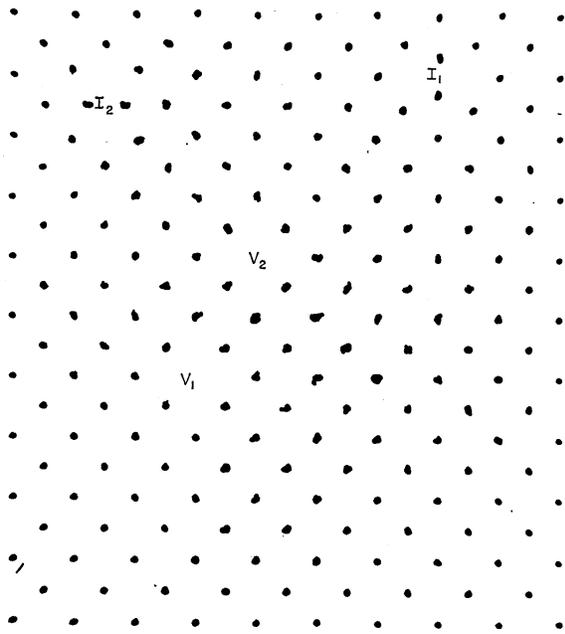
FIG. 24. Same event shown in Fig. 23, orbits from time 200 to 703. Two vacancies, V_1 and V_2, and two stable interstitials, I_1, and I_2 have formed.

two interstitials, at the somewhat distant points I_1 and I_2 (see Fig. 24). Twelve replacements are seen. Figure 24 shows the same plane from the time where Fig. 23 was terminated up to time 704. The defect pattern is now well established and the atomic vibrations are all quite restricted. Vacancies and interstitials are marked by the same symbols as in Fig. 23. Figure 25(a) (Run No. 97) shows orbits produced by a 400-ev knock-on atom, directed initially 10° away from [011]. The knock-on atom started at K and goes to K'. This shot runs to time 45, at which time large motions have reached the boundary and the configuration is still rather far from equilibrium.

The 400-volt event in Fig. 25 really exceeds the capabilities of our present computing methods. It is presented, however, as a suggestive example of intermediate energy damage events. By looking at the energies of key orbits at the end of this run and drawing on experience gained with lower energy shots, it is possible to estimate the final configuration. This estimate is no more than a plausible guess, and many of its particular features are likely to be revised when more powerful computing methods become available. The general character of the damage may, however, be correctly assessed. The action remaining at the end of the calculation is analyzed into a number of collision chains. $\langle 100 \rangle$ chains are still active at A, B, C, D, E, F, G, and H. Looking at the kinetic energies at these points and using the rule that a focused $\langle 100 \rangle$ chain loses about 7 ev per step, one estimates that 8 interstitials would eventually be formed at sites outside the fundamental

set, as indicated in Fig. 25(b). In addition 3 interstitials appear to be forming inside the set, at sites also indicated in Fig. 25(b). A total of 11 vacancies must also have been produced; the sites of some of these are obvious, others are found by extrapolation, and these locations are indicated by open circles in the figure. About 39 replacements are estimated to occur. It is quite possible that some of these closely spaced vacan-

(a)

(b)
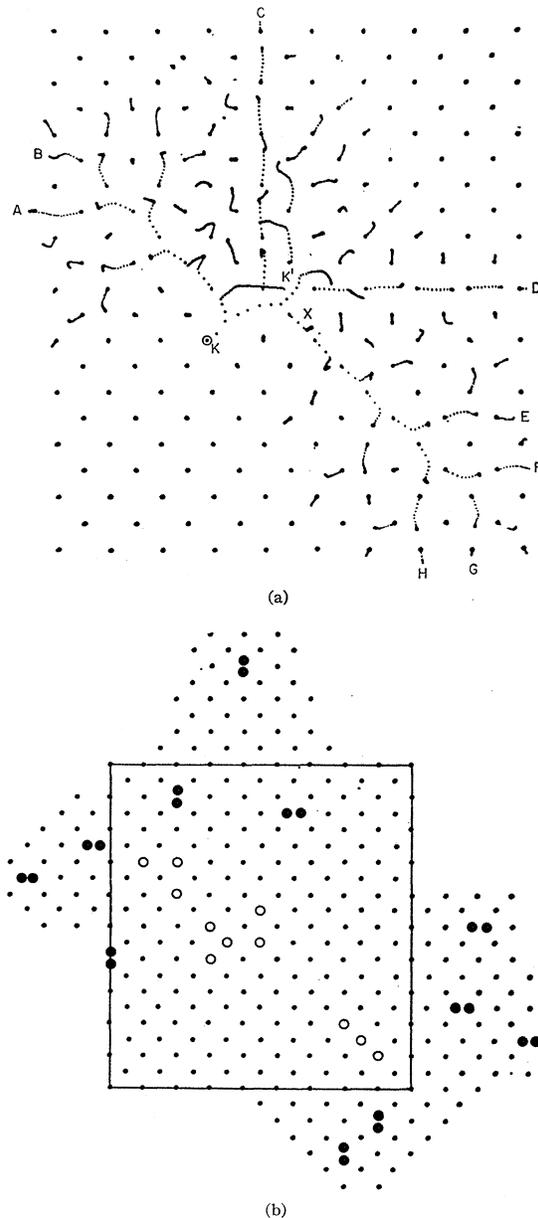
FIG. 25. (a) Shot in (100) plane at 400 ev, 10° away from [011]. Orbits in plane to time 45 are shown. Knock-on started at K, moves to K'. At end of run collision chains $A,B,\cdots H$ are still active (Run No. 97). (b) Estimated array of 11 vacancies (circles) and 11 interstitials (double dots) that could result from shot in Fig. 25(a). Set used in Fig. 25(a) indicated by rectangle. Indicated vacancy arrangement may not be stable.

cies will immediately rearrange themselves (as, for example, in the case of a closely spaced trivacancy[25]), but it is not possible to make any reliable statements about this yet.

The configuration of vacancies and interstitials produced is noteworthy for several reasons. The vacancies are near the site of the original knock-on, the interstitials are farther away. $\langle 110 \rangle$ collision chains have not played as prominent a role in this event as in some of the lower energy events discussed earlier. This can be attributed to the fact that the energies here are far above the focusing limit for $\langle 110 \rangle$ chains, causing these to spray out into $\langle 100 \rangle$ chains which are near or below their focusing threshold. An especially clear example is the chain which starts at X and moves toward the lower right corner of the figure. The kinetic energy at X is 125 ev. The action along this line is reminiscent in many ways of Brinkman's displacement spikes,[1] although there is nothing like the melting and turbulent mixing that he predicted. Note especially the 3 vacancies in a line and the 5 interstitials outside them. It seems clear that, at this energy, almost every kind of stable cluster of vacancies and interstitials will be produced, at least when there is even the slightest annealing.

Shots 96 and 97 had the same starting velocities in the large set C as shots 62 and 63, respectively, had in the smaller set B (see Appendix). The latter two shots could not be run to completion, because of boundary limitations, (No. 62 ran very nearly to completion) but the individual orbits in 62 coincided almost exactly with the corresponding orbits in 96, and those in 63 agreed very closely with the corresponding orbits in 97. This gave further evidence that boundary conditions are not seriously disturbing our results.

B. Collision Chains

One of the most striking features of the orbital plots reported here is the strong tendency of energy to propagate along two preferred lines of atoms, the close packed $\langle 110 \rangle$ lines, and the cubic $\langle 100 \rangle$ lines. As mentioned before, the $\langle 110 \rangle$ effect was anticipated by Silsbee, who first pointed out that focusing occurs in an isolated, uniformly spaced straight line of hard spheres. Figure 26 shows such a line. If the first sphere is projected toward the second at an angle θ_1 with the line of centers, the second will be driven away at an angle θ_2, given by

$$\theta_2 = \sin^{-1}[(S/D \sin\theta_1)] - \theta_1, \qquad (21)$$

where S is the separation of centers and D is the diameter of a sphere. If the spheres are sufficiently closely spaced θ_2 will be less than θ_1, and in general θ_{i+1} will be less the θ_i. If θ_1 is small, Eq. (21) reduces to

$$\theta_2 = (S/D - 1)\theta_1, \qquad (22)$$

and focusing occurs if $S/D < 2$. For atoms that are soft spheres, a first approximation is obtained if an equi-
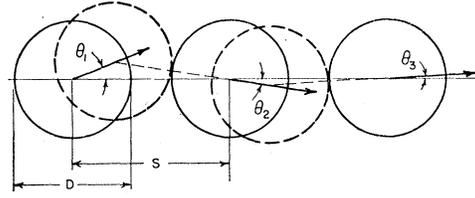
Fig. 26. Hard sphere collision chain.

valent hard-sphere diameter is defined, equal to the distance of closest approach of the atoms in a head-on collision. Considering a moving atom with kinetic energy E to be in collision with a stationary atom of equal mass, and using the exponential repulsive potential

$$\varphi = Be^{-\beta r},$$

one finds the hard-sphere diameter for energy E to be

$$D = (1/\beta) \ln 2B/E. \qquad (23)$$

The strength of the focusing can be conveniently described by a focusing parameter Λ defined as the ratio of angles θ_2 and θ_1:

$$\Lambda = \theta_2/\theta_1. \qquad (24)$$

For small angles, one has from (22)

$$\Lambda = (S/D) - 1, \qquad (25)$$

with D given by Eq. (23).

In a more realistic model, as employed in the present calculations, the row of atoms is not isolated, but is embedded in adjoining rows of atoms. Also a moving atom is in continuous interaction with its next neighbor in the line, and it is not possible to make a rigorous separation of the collision into before and after stages: the moving atom pursues a curved trajectory, losing speed continuously, and the struck atom moves away on a curved trajectory as it gradually picks up speed. It is thus of considerable interest that the calculations produce collision sequences having such close qualitative resemblances to the Silsbee chains. In order to check more closely on the resemblance, and also in order to see if the focused chains observed can be easily characterized so that complex damage events can be resolved into simple elements, a quantitative study has been made of the chains appearing in our calculations. A chain was characterized in the ith stage ($i = 1, 2, 3, \ldots$) by a kinetic energy E_i and by the angle θ_i between the axis of the chain and a tangent to the orbit of the moving atom. E_i was always chosen as the kinetic energy of one atom, at the point of its maximum kinetic energy, and θ_i was also defined at this point[27]; this seemed to be the best compromise between the require-

[27] θ_i was taken to be the angle between the axis of the chain and the velocity vector of the moving atom at its point of maximum kinetic energy. This is nearly, but not quite, the same as the angle between the axis of the chain and a line running from the original site of the atom to its point of maximum kinetic energy.

ments that the preceding collision be ended and the next collision not yet begun. If the angle in the chain at its next stage is θ_{i+1}, it is convenient to define a focusing parameter $\Lambda(E_i)$ as

$$\Lambda(E_i) = \theta_{i+1}/\theta_i. \tag{26}$$

Examining the major $\langle 110 \rangle$ focusing chains occurring in all of our calculations with interatomic potential 2, and limiting attention to cases where θ_i was less than 20° and did not belong to a boundary atom, values of $\Lambda(E)$ for a large variety of energies E were found. These points are plotted in Fig. 27, and are seen to lie on a rather well defined curve. Very little dependence of Λ on θ was observed, and most of the scatter of the points in the figure can be attributed to the somewhat arbitrary attempt to characterize chains initiated in a variety of ways by only two parameters, θ and E, and also, to a minor extent, to truncation error. From Fig. 27 it is seen that $\Lambda = 1$ at $E \cong 30$ ev, so that chains above 30 ev are defocused, chains below 30 ev are focused. A defocused chain increases its angle and causes a more rapid loss of energy. In $\langle 110 \rangle$ chains, the energy lost at each stage is found to be approximately

$$\Delta E_i = \tfrac{2}{3}(\text{ev}) + E \sin^2(\theta_i + \theta_{i+1}). \tag{27}$$

As the angle increases, the attrition of energy increases until the chain drops into the focusing range. Its angle then rapidly approaches zero and the chain continues for a distance determined by the first term in Eq. (27). This term arises because even the perfectly focused chain must force its way between neighbors and lose some energy to them. The value 2/3 ev per step was found to be a fairly good approximation for repulsive potential 2 at small angles and for chain energy E between about 3 and 400 ev.

Using Eq. (23) for D in Eq. (25) one has what may be called the modified hard sphere approximation. This result is also plotted in Fig. 27, again for repulsive potential 2, and is seen to overestimate the true degree of focusing.
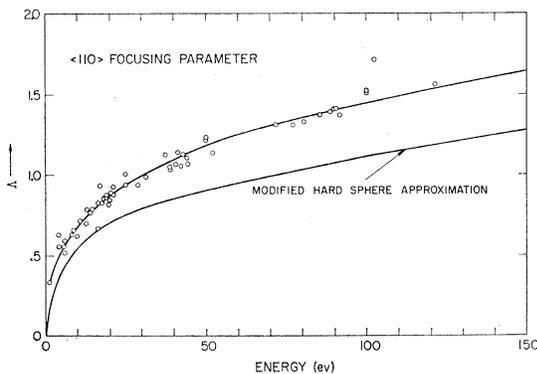
The number of replacements occurring in a chain that starts with energy E_1 and angle θ_1 can now be calculated. Taking $\Lambda(E_1)$ from the solid line through the "experimental" points in Fig. 27, one finds the second angle in the chain, θ_2, from $\theta_2 = \Lambda(E_1)\theta_1$. Then using Eq. (27) to find the energy loss ΔE_1 one has the second energy in the chain

$$E_2 = E_1 - \Delta E_1.$$

The process is now repeated, starting with E_2 and θ_2, to find energy and angle in the third stage of the chain; by iteration, energy and angle at each successive stage are found. From the dynamic events run to date it is estimated that a well-focused chain produces an interstitial (and thus ceases to transport matter) when its energy falls to about 3 or 4 ev. This energy is subject to rather wide limits of error, in the present stage of our computa-
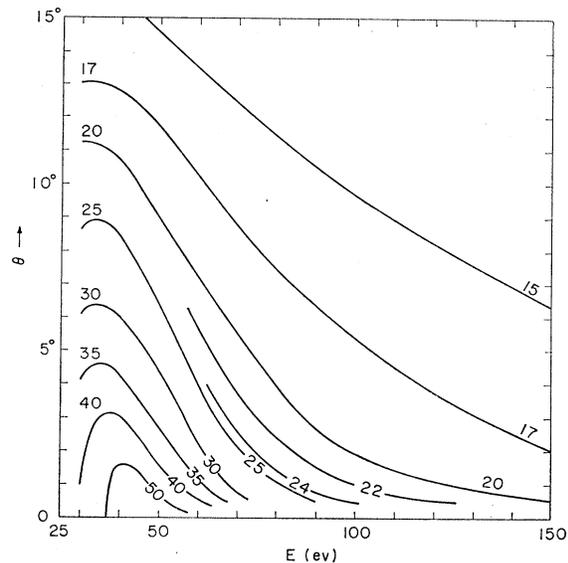
FIG. 28. Calculated lengths N of $\langle 110 \rangle$ collision chains started at various angles and energies. See Sec. 5B.

tions, but will be assumed to be 3.5 ev for the present purpose. A quantity $N(E,\theta)$ is defined as the number of collisions required for the energy of a chain that starts at energy E and angle θ (assuming $E \gtrsim 30$ ev and $|\theta| < 15°$) to drop to 3.5 ev. This quantity, $N(E,\theta)$, is the number of replacements in the chain, and it also is the distance (in atomic spacings) between the vacancy at the start of the chain and the interstitial at its end. Contours of constant $N(E,\theta)$ are shown on a plane of E and θ in Fig. 28. It is seen that the length of a chain initiated at low energies (around 50 ev) diminishes rather slowly as θ increases, while the length of a higher energy chain drops very rapidly as θ increases. Along the line $\theta = 0$, $N(E,\theta) = \tfrac{3}{2}(E-3.5)$. This predicts that a 100-volt chain with $\theta = 0$ travels 146 atomic spaces, while a 100-volt chain with $\theta = 1°$ travels only 22 spaces. It is obvious that the considerations leading to Fig. 28

FIG. 27. Focusing parameter $\Lambda = \theta_2/\theta_1$, as found from $\langle 110 \rangle$ chains in various runs (open circles).

are quite crude, but it is felt that the figure represents a better approximation than earlier work based on a hard-sphere model. The contours in Fig. 28 are terminated at 30 ev because the assumptions in their derivation do not apply to chains initiated at energies lower than this.

It is noteworthy that an appreciable fraction of the total energy in a $\langle 110 \rangle$ chain resides, at any time, as potential energy of compressed bonds in the chain. This potential energy is a minimum when the kinetic energy of the atom at the center of a pulse is a maximum, and reaches a maximum one half cycle later. In the chain initiated at 25 ev (No. 40) the minimum of potential energy is about 3 ev and the maximum is about 10 ev; in the chain initiated at 100 ev (No. 44) the minimum is about 6 ev, the maximum about 45 ev; in the chain initiated at 400 ev (No. 45) the minimum is about 12 ev, the maximum about 195. The average potential energy is approximately the mean of the minimum and the maximum. This behavior is very different from that of the chain of hard spheres, where the average potential energy is zero. Also the storage of potential energy is associated with a drop in the maximum kinetic energy between the initial stage and the second stage, and Eq. (27) does not apply to the energy loss in the initial stage. The struck atom must supply the chain's potential energy from kinetic energy, and thus the maximum kinetic energy of the second atom (when $\theta = 0$) is less than the knock-on kinetic energy by approximately 2/3 ev plus the minimum value of the potential energy of the chain.

The $\langle 100 \rangle$ lines are more widely spaced than the $\langle 110 \rangle$ lines by a factor $\sqrt{2}$. A modified hard-sphere theory for these lines would predict defocusing at all energies above 5.5 ev. Much stronger focusing effects are actually observed in these lines, and examination of Fig. 6 shows that this occurs because of the confining action exerted by neighboring lines: it is quite insufficient to consider a $\langle 100 \rangle$ line to be isolated. Focusing in a variety of $\langle 100 \rangle$ chains in our calculations (all for interatomic potential 2) was examined, and characterized at each stage by a parameter Λ, defined exactly as for the $\langle 110 \rangle$ chains [Eq. (26)]. The results are presented in Fig. 29. Again there is some scatter of points, attributable to the same causes. Focusing occurs, in general, when the kinetic energy is less than about 40 ev, and defocusing occurs at energies above this. As energy increases above the focusing threshold, Λ grows more rapidly in the $\langle 100 \rangle$ case than in the $\langle 110 \rangle$ case. The angles θ range up to 20° for the events represented in Fig. 29, but the majority of angles are below 3°. As with $\langle 110 \rangle$ chains, no systematic dependence of Λ on θ could be found within the range examined.

All of the chains represented in Figs. 27 and 29 lay in $\{100\}$ planes.[28] Since $\langle 110 \rangle$ is a twofold axis, chains

[28] The plane in which a collision chain is said to lie is defined by the axis of the chain and the velocity of an atom at the center chain.
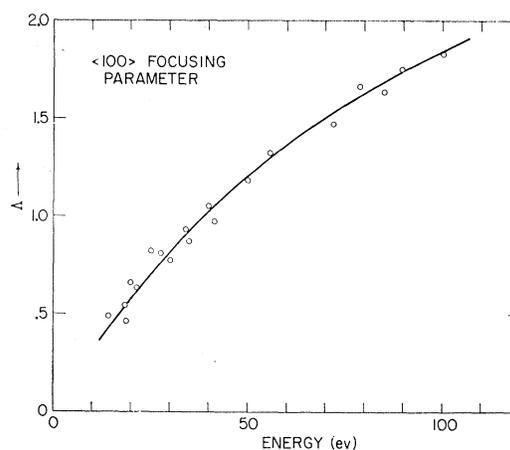
FIG. 29. Focusing parameter $\Lambda = \theta_2/\theta_1$, as found from $\langle 100 \rangle$ chains in various runs (open circles).

along this axis but not lying in a $\{100\}$ plane need not behave exactly like those determined. However, for small and moderate angles θ (up to perhaps 15°) $\langle 110 \rangle$ chains are highly independent of their surroundings, and thus all $\langle 110 \rangle$ chains at small angles, regardless of the plane in which they lie, should focus about as indicated in Fig. 27. The $\langle 100 \rangle$ chains, as has been pointed out, are not independent of their surroundings, indeed require them for focusing. However, the $\langle 100 \rangle$ axes have fourfold rotational symmetry. This requires that, to second order in θ, a $\langle 100 \rangle$ chain is also independent of the orientation of the plane in which it lies.

A simple theory of assisted focusing can be constructed using the impulse approximation to treat the glancing collision with the $\langle 110 \rangle$ neighbor and a modified hard-sphere model for the nearly head-on collision with the $\langle 100 \rangle$ neighbor down the chain. This has been done by the writers and independently by Thompson and Nelson.[29] The impulse approximation gives a focusing parameter which rises with energy very much like the curve of Fig. 29, but which is too low at every point. In our version of the impulse approximation the threshold energy, below which $\langle 100 \rangle$ focusing would be expected, is 84 ev, and in the form of Thompson and Nelson it is 74 ev, in contrast with the value 39 ev found from the present machine calculations. A large part of the discrepancy can be blamed on failure of the impulse method at these rather low energies. A more accurate analytical treatment would appear to be rather complicated.

C. Number of Defects Produced

Let us return now to Fig. 5 where the results of all shots made to date with interatomic potential 2 are represented as points in a plane. Plotted vertically is the initial kinetic energy of the shot, and horizontally the angle between the initial velocity of the knock-on and

[29] We are indebted to Dr. Thompson for informing us of his results before publication.

the $\langle 100 \rangle$ axis. In the left portion of the figure are cases with initial velocities lying in the {110} plane, and in the right portion are cases with initial velocities in the {100} plane. Each shot is represented by a point and attached to most points are two numbers. The first number gives the number of atoms permanently displaced to interstitial positions by the shot; the second figure (in parentheses) gives the number of atomic replacements occurring in the shot. In some cases one or both of these numbers had to be estimated by a substantial extrapolation, and in such cases a question mark is affixed. In four cases no extrapolation sufficiently reliable to report could be made. In these no numbers are given. Points on the left and right edges of the figure are the same, both edges being $\langle 110 \rangle$ axes. The dotted line gives an estimate, from these points and from general considerations, of the threshold energy, at each angle, for producing a permanent displacement. The $\langle 110 \rangle$ threshold is assumed, somewhat arbitrarily, to be 28 ev, and the $\langle 100 \rangle$ threshold is shown as 24 ev. Lattice symmetry requires this line to have zero slope at $\langle 110 \rangle$, $\langle 111 \rangle$, and $\langle 100 \rangle$. The thresholds on these axes are fairly well determined, but considerable uncertainty prevails in several regions.

It is clear from Fig. 5 that for most directions the threshold for producing a replacement lies well below the threshold for displacement, and the number of replacements is generally much larger than the number of displacements. From the data presented, some remarks can be made about the important quantity $p(E)$, defined as the probability of producing at least one displacement, starting with a knock-on of kinetic energy E and of random direction. The probability $p(E)$ rises from zero at 24 ev, and becomes unity at about 85 ev. From considerations of the symmetry of the fcc lattice, one can show that the curve of $p(E)$ versus E must commence with a finite slope and must reach 1 with a finite slope. It must also have at least three more discontinuities of slope between these discontinuities, in the lowest of which three the slope increases discontinuously with increasing E and in the highest of which three the slope decreases discontinuously with increasing E. The effects of quantum mechanics and thermal vibrations, however, probably would round off these discontinuities and make them unobservable. A straight line rising from zero to one in the interval $E=24$ ev to $E=85$ ev should be a reasonably good approximation to $p(E)$ as indicated by the present calculations with potential 2.

Of more direct interest is the average number of permanent displacements $\nu(E)$ produced by a knock-on atom with kinetic energy E and random direction. The results presented in Fig. 5 allow the conclusion that $\nu(E)$ equals 0 for E less than 24 ev, and rises at about this point with a finite slope, not reaching unity until E is considerably above 24. Unfortunately the calculations completed to date provide too small a sample of directions and energies of the knock-on to give much of a

curve of $\nu(E)$. From the fact that two displacements were not produced in any shot below 100 ev, and at this energy in only one out of 5 examples, it is plausible that $\nu(E)$ reaches 1 between 80 and 90 ev. The curve of $\nu(E)$ versus E will contain all the discontinuities of slope of $p(E)$ plus many more at higher energies. Again it is questionable whether these would exist in a model taking account of thermal motions and quantum effects.

6. SUMMARY AND CONCLUSIONS

The calculations presented here give a more intimate view of radiation damage events at low and moderate energies in a face-centered cubic metal than has been obtained before. It should be remembered, however, that all results are based on a simple model of metallic copper which is plausible, but whose accuracy has not been finally established. With this reservation, the following conclusions concerning radiation damage and lattice defects in copper have been reached:

1. Damage at low energies consists of vacancies and interstitials. This point is only confirmation of what has been commonly supposed.

2. Vacancies are of the conventional character, but interstitials reside in the split configuration (Fig. 3); no other configuration of the interstitial has been found to be stable.

3. The regular arrangement of atoms on a lattice has an important influence on the character of damage events. Collision chains occur in both $\langle 110 \rangle$ and $\langle 100 \rangle$ directions, propagating with especially low loss of energy in the former direction, as anticipated by Silsbee.[26] Chains in $\langle 110 \rangle$ focus at kinetic energies below approximately 30 ev, chains in $\langle 100 \rangle$ focus below 40 ev; all chains defocus at higher energies. These thresholds are surprisingly low.

4. A chain with energy above 25 or 30 ev carries matter, as well as energy, somewhat in the fashion of the "dynamic crowdion,"[8] and produces an interstitial atom near its terminus. The ranges of various $\langle 110 \rangle$ chains have been estimated (Fig. 28).[30]

5. Because of the "dynamic crowdion" action interstitials tend to be produced at a distance from the site of a primary knock-on, while the vacancies, having no mechanism of propagation, remain behind in fairly compact groups. At moderate energies a variety of clusters of vacancies, and possibly more complex configurations resulting from the collapse or rearrangement of such clusters, can be expected. The present calculations have not yet been able to follow such rearrangements in detail. The question of the existence of amorphous zones at the site of a damage event, as suggested by Seeger,[7,8] is not yet settled.

6. Another result of the collision chains is the production of many more replacements than displacements. In

---

[30] See also G. Leibfried, J. Appl. Phys. **30**, 1388 (1959); **31**, 117 (1960). Our conclusions about focusing chains are somewhat different from Leibfried's.

compounds or alloys of nearly homogeneous mass this effect would produce many more disordered atoms than displaced atoms.[31]

7. The threshold energy for producing a single Frenkel pair is lowest (about 25 ev) in or near $\langle 100 \rangle$ and probably is almost as low in or near $\langle 110 \rangle$. The threshold is much higher, probably 85 ev, around $\langle 111 \rangle$. Experiments on the directional dependence of the threshold are clearly indicated.

8. The closest Frenkel pairs are not stable, in the present model, and pairs along $\langle 110 \rangle$ directions must be separated to 4th neighbor positions in order to be stable (see Fig. 4). These conclusions are probably rather sensitive to the details of the force law employed.

9. Knock-ons with energy near threshold produce a variety of Frenkel pairs. The explanation advanced by Corbett, Smith, and Walker[4] for the substages that they observed in the lowest temperature annealing of electron irradiated copper are consistent with results reported here, except that the interstitial is not in the position assumed by Corbett et al., and the present calculations are not far enough advanced to identify particular Frenkel pairs with all of the particular annealing substages. In further work is it hoped that such identification, which would constitute a sensitive check on the model, can be made. Corbett and Walker[32] have also studied the effect on the annealing spectrum of varying the bombardment energy, and find that lowering the bombardment energy appears to decrease the number of distant pairs relative to the number of closer pairs by a surprisingly small amount. This phenomenon finds ready explanation in the calculations reported here—the $\langle 110 \rangle$ threshold appears to be very

little, if any, above the $\langle 100 \rangle$ threshold, and yet $\langle 110 \rangle$ displacement events, through dynamic crowdion action produce interstitials at a considerable distance from the vacancy, while $\langle 100 \rangle$ displacement events produce the interstitial relatively close by. Varying the maximum energy of knock-ons from 115 ev to 37 ev, as Corbett and Walker have done, would thus produce rather little change in the relative number of distant ($\langle 110 \rangle$ type) and close ($\langle 100 \rangle$) type Frenkel pairs.

10. Agitations following damage events of moderate energy are seen to bear some resemblance to thermal spikes (see Figs. 9 and 10), but the transport of energy is far from isotropic, as would be predicted by thermal-spike models in a cubic material. Localized vibrational modes associated with interstitials are prominently excited, and retain their energy longer than other modes. Localized annealing appears to be promoted by the excitation that lingers in these modes.

11. It would appear that these calculations have proved the feasibility of simulating events of radiation damage by mathematical models on high speed computers. Limitations on the size of the set of atoms that can be treated are still a matter of concern, and practical means of increasing this size are under study. Further checks and improvements on the force laws are needed. Work in these areas is continuing.

[31] G. H. Kinchin and R. S. Pease [Reports on Progress in Physics (The Physical Society, London, 1955), Vol. 18, p. 1] suggested the importance of replacements, although their treatment bore little resemblance to the results of our calculations.

[32] J. W. Corbett and R. M. Walker, Phys. Rev. 115, 67 (1959).